Roles of P-body factors in *Candida albicans* filamentation and stress response

Melissa A. Tosiano[1], Frederick Lanni[1], Aaron P. Mitchell[2], C. Joel McManus[1]*

1 Department of Biological Sciences, Carnegie Mellon University, Pittsburgh, Pennsylvania, United States of America, **2** Department of Microbiology, University of Georgia, Athens, Georgia, United States of America

*Corresponding author

mcmanus@andrew.cmu.edu

Abstract

Hyphal growth is strongly associated with virulence in the human fungal pathogen *Candida albicans*. While hyphal transcriptional networks have been the subject of intense study, relatively little is known about post-transcriptional regulation. Previous work reported that P-Body (PB) factors Dhh1 and Edc3 were required for *C. albicans* virulence and filamentation, suggesting an essential role for post-transcriptional regulation of these processes. However, the molecular roles of these factors have not been determined. To further study the function of PB factors in filamentation, we generated homozygous deletions of *DHH1* and *EDC3* in diverse prototrophic clinical strains using transient CRISPR-Cas9. Homozygous *DHH1* deletion strongly impaired growth, altered filamentation, and exhibited unusual colony morphology in response to heat stress in five strain backgrounds. Using RNA-seq, we found *DHH1* deletion disrupts the regulation of thousands of genes under both yeast and hyphal growth conditions in SC5314 and P57055. This included upregulation of many stress response genes in the absence of external stress, similar to deletion of the *S. cerevisiae DHH1* homolog. In contrast, we found *EDC3* was

not required for heat tolerance or filamentation in diverse strains. These results support a model in which *DHH1*, but not *EDC3*, represses hyphal stress response transcripts in yeast and remodels the transcriptome during filamentation. Our work supports distinct requirements for specific mRNA decay factors, bolstering evidence for post-transcriptional regulation of filamentation in *C. albicans*.

Author summary

In the dimorphic fungal pathogen *C. albicans*, the hyphal phenotype strongly correlates with pathogenicity. While transcriptional control of hyphal growth has been extensively studied, comparatively little is known about post-transcriptional regulation of this significant morphological shift. PB factors are associated with mRNA decay and translational repression. Here we investigate the roles of two PB factors in growth, filamentation, and gene expression. Although deletion of PB factor *EDC3* did not impact growth or filamentation, *dhh1Δ/Δ* had greatly impaired growth and heat tolerance as well as unusual hyphal phenotypes in multiple clinical isolate strains. Additionally, we found that the transcriptomes of SC5314 and P57055 *dhh1Δ/Δ* yeast and hyphae were highly dysregulated. The extensive transcriptomic impacts of the absence of Dhh1 correlated with our phenotypic findings. Stress-associated genes were induced under non-stress conditions and the filamentation response was blunted under physiologically relevant *in vitro* conditions. We demonstrate that mRNA decay factors play distinct roles in regulating *C. albicans* morphology and that Dhh1 contributes to environmentally appropriate expression of the stress response and hyphal growth.

Introduction

Candida albicans is an opportunistic pathogen that causes blood and deep tissue infections (candidiasis) in immunocompromised individuals [1, 2]. Pathogenicity requires responding to stress in divergent physiological microenvironments [3, 4]. Under stress, *C. albicans* undergoes

filamentation, shifting from commensal yeast to virulent hyphae. Hyphal growth correlates with the release of the peptide toxin candidalysin [5] and adherent biofilm formation [6–8]. Both contribute to pathogenicity. Foundational research on transcriptional regulation of filamentation identified dozens of transcription factors (TFs) and signaling cascades controlling core filamentation response networks [9–12]. Under different hyphal-inducing conditions, *C. albicans* activates distinct transcriptional programs [13]. Notably, these transcriptional programs have been found to vary dramatically across different clinical isolates, even under the same filamentation conditions [14]. Despite deep exploration into transcriptional control of filamentation, comparatively little work has addressed post-transcriptional regulation of filamentation [15, 16].

Eukaryotes implement swift and precise post-transcriptional stress responses [17, 18] appropriate for regulating the acute stage of *C. albicans* filamentation [15, 16]. Post-transcriptional regulation of gene expression integrates mRNA translation, localization, and decay [19, 20]. Indeed, mRNA decay has been found to regulate adaptation to the host environment and virulence in several human fungal pathogens [3, 16, 21, 22]. Localization to ribonucleoprotein (RNP) granules represses translation and initiates decay in many organisms [23, 24]. P-bodies (PBs) are RNPs associated with the Ccr4-not deadenylase complex [24–27] and mRNA degradation [23, 24, 28]. In *C. albicans*, several PB mRNA decay factors have been reported to function in hyphal development and virulence, including Ccr4, Pop2, Not5, Xrn1, Dhh1, and Edc3 [29–37]. However, all of these studies used auxotrophic derivatives of SC5314 such as BWP17 and CAI4, therefore it is unknown how important these factors are in clinical isolates. In addition, the effects of these factors on gene regulation during filamentation have not been elucidated.

Stochastic transcriptional noise generates different phenotypic outcomes in clonal microbial populations that serves as a mechanism of “bet-hedging” for acute environmental stressors [38–40]. In this context, mRNA decay provides a system of transcript buffering preventing gene

73 expression under inappropriate conditions [41]. Genes identified as both transcriptionally noisy
74 and poorly translated have these features conserved between *S. cerevisiae* and *C. albicans*
75 homologs [42]. However, the extent to which mRNA decay factors buffer or control noisy
76 expression of hyphal genes under yeast-form conditions or conversely yeast genes under
77 hyphal conditions remains unclear in *C. albicans*. Furthermore, the roles of *C. albicans* PB
78 factors in buffering noisy transcription for environmentally appropriate gene expression remain
79 unknown.

80 In the model yeast *S. cerevisiae*, the functions of PB factors Dhh1 and Edc3 have been
81 extensively studied [43]. The DEAD-box helicase and activator of mRNA decapping Dhh1
82 rapidly exchange between the cytoplasm and PBs [44, 45], and may repress translation and
83 stimulate the decay of mRNAs with poor codon optimality [46, 47]. Under optimal growth
84 conditions it has been reported that Dhh1 represses genes associated with nutrient limitation,
85 cell wall components, autophagy, and metabolism of non-preferred carbon and nitrogen sources
86 [48]. Loss of *DHH1* in *S. cerevisiae* downregulates *STE12* translation leading to defects in
87 pseudohyphal growth and mating [35, 49, 50], and the *C. neoformans* Dhh1 homolog (Vad1)
88 plays a similar role in regulating mating [51]. Kinase signaling via Dhh1 phosphorylation sites
89 are critical to pseudohyphal development in *S. cerevisiae* [35, 52]. Edc3 is a non-essential
90 enhancer of mRNA decapping and a PB scaffolding factor in *S. cerevisiae* [43, 44, 53, 54]. In *S.*
91 *cerevisiae*, the absence of Edc3 reduces PB assembly size, but does not impede global mRNA
92 decay [44, 55]. Additionally, Edc3 is dispensable for PB formation in *S. pombe* [56]. In contrast
93 to *S. cerevisiae*, the roles of Dhh1 and Edc3 in *C. albicans* hyphal growth have been minimally
94 explored and the impact of Dhh1 on gene expression remains unknown.

95 Prior work in *C. albicans* reported that both Dhh1 and Edc3 are necessary for WT stress
96 tolerance and filamentation. In a *C. albicans* auxotrophic background, the authors described a
97 heterozygous deletion of *DHH1* (*DHH1/dhh1Δ*) which produced WT colonies on YPD plates, but

98 was filamentation impaired [35]. In the same *C. albicans* auxotrophic background, *edc3Δ/Δ* was
99 noted to have compromised PB condensation, reduced heat tolerance at 37°C, and severely
100 restricted filamentation [36, 37]. This early research implied that *DHH1* and *EDC3* may have
101 distinct roles in *C. albicans* filamentation. However, the gene regulatory effects of *DHH1*
102 deletion in *C. albicans* have not been defined. Thus, our understanding of these important PB
103 factors in filamentation remains limited.

104 In this study, we investigated the roles of PB factor Dhh1 in *C. albicans* heat tolerance,
105 filamentation, and gene expression. Using transient CRISPR-cas9 [57] we deleted *DHH1* and
106 *EDC3* in diverse clinical isolate strains representing the five major *C. albicans* clades [58]. We
107 demonstrated the dispensability of *EDC3* for PB condensation, heat tolerance, and
108 filamentation. Importantly, we found *dhh1Δ/Δ* exhibits impaired yeast-form growth, heat
109 sensitivity, and anomalous filamentation across genetic backgrounds. Finally, we determined
110 the effects of *dhh1Δ/Δ* on genome-wide expression in yeast and early hyphae, and found loss of
111 *DHH1* causes widespread dysregulation of the transcriptome and stress responses in SC5314
112 and P57055.

113 Results

114 Characterizing P-Bodies (PBs) in *C. albicans*

115 To investigate the presence of Dhh1 and Edc3 in PBs, we first fused mScarlet to the C-terminus
116 of Dhh1 (Dhh1-mS) and mNeonGreen to the C-terminus of Edc3 (Edc3-mNG) using CRISPR-
117 Cas mediated genome editing in strain SC5314. Under optimal temperature and acute heat
118 shock, Edc3-mNG condensed into round foci (Fig 1. A-B). To determine if these foci were PBs,
119 we generated a dual labeled strain (Edc3-mNG, Dhh1-mS). Edc3-mNG and Dhh1-mS
120 colocalized, confirming these foci were PBs (Fig 1. C, Fig S1. A). As is the case in *S. cerevisiae*
121 [59], we found a large fraction of Dhh1 was cytoplasmically diffuse, suggesting it functions both

122 in PBs and in the cytoplasm (Fig 1. C, Fig S1. A). We next investigated PB condensation during

123 early filamentation. After 3 hours of acute glucose starvation in PBS, PBs were abundant in

124 yeast cells and along developing hyphal germ tubes (Fig 1. D). PBs also formed and persisted

125 over 4 hours of filamentation (37°C and RPMI), (Fig 1. E). Lastly, we investigated whether these

126 proteins were independently required for PB condensation. In the absence of Edc3, Dhh1-mS

127 retained the capacity to form condensates in response to acute heat shock (Fig 1. F, Fig S1. B).

128 Similarly, Edc3-mNG also condensed in the absence of Dhh1 (Fig 1. G, Fig S1. C). In summary,

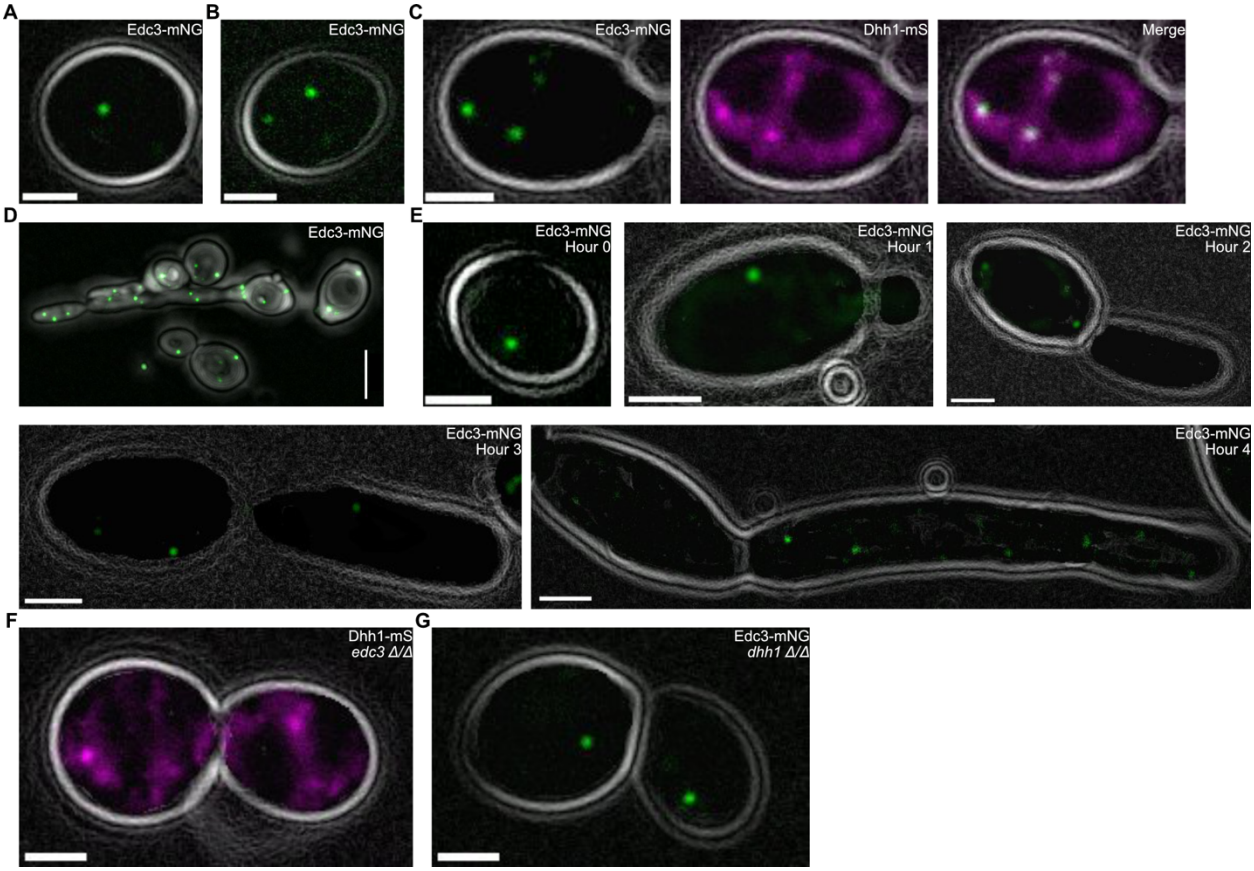

Figure 1. PBs condense during acute stress. Images of PB factors fluorescently tagged in strain SC5314. **A.** Edc3-mNG condensed in live *C. albicans* under non-stress conditions (30°C in complete media (CM)). Scale bar = 5μm. **B.** Edc3-mNG condensed in live *C. albicans* in response to acute heat shock (10 minutes at 46°C in CM). Scale bar = 5μm. **C.** PB factors (Edc3-mNG and DHH1-mS) co-localized during acute heat shock (10 minutes at 46°C in CM) confirming their identity as PBs. Scale bar = 2μm. **D.** After 3-hours of starvation in PBS at room temperature, abundant PBs (Edc3-mNG) were visible with confocal microscopy along the developing germ tube. Scale bar = 5μm. **E.** PBs (Edc3-mNG) also condensed and persisted during hyphal growth (37°C in RPMI). Scale bars = 2μm. **F.** Dhh1-mS condensed in the absence of Edc3 in response to acute heat shock (10 minutes at 46°C in CM). Scale bar = 2μm. **G.** Dhh1 is not required for Edc3-mNG PB formation in response to acute heat shock (10 minutes at 46°C in CM). Scale bar = 5μm.

129 we confirmed the presence of PBs in *C. albicans* and found that, as in *S. cerevisiae*, *C. albicans*
130 PBs are robust condensates tolerating the absence of Dhh1 or Edc3 individually.
131

132 **_DHH1_ is required for normal growth and stress response phenotypes in SC5314**

133 We next investigated the role of Dhh1 and Edc3 in *C. albicans* growth and stress responses.
134 We generated heterozygous (*DHH1*/*dhh1Δ*) and homozygous (*dhh1Δ/Δ*) *DHH1* deletions and
135 complements in SC5314. Initially, we conducted spot assays at 30°C and 37°C to test for
136 growth and temperature sensitivity defects. Strains possessing at least one copy of *DHH1*
137 produced colonies identical to WT on YPD plates (Fig 2. A-B). However, *dhh1Δ/Δ* had impaired
138 growth across timepoints and incubation temperatures (Fig 2. A-B). We also observed slow
139 growth of *dhh1Δ/Δ* at 30°C in liquid YPD over 12 hours (Fig 2. C). Uniquely, after 3 days on
140 YPD at 37°C, *dhh1Δ/Δ* colonies exhibited a wrinkled appearance associated with hyphal growth
141 (Fig 2. B). To further investigate, we grew colonies at 37°C for 4 days on YPD. While strains
142 with *DHH1* had a smooth surface and soft texture, *dhh1Δ/Δ* colonies had a wrinkled surface and
143 firm, dry texture reminiscent of hyphal colonies on spider media (Fig 2. D). Surprisingly, DIC
144 microscopy revealed *dhh1Δ/Δ* cells were twice the size of the *DHH1*-containing strains, with
145 enlarged vacuoles (Fig 2. E). The size of the cells (Fig 2. F), vacuoles (Fig 2. G), and proportion
146 of the cell taken up by the vacuole (Fig 2. H) were all significantly greater in *dhh1Δ/Δ* cells. The
147 slow growth and altered cell physiology of *dhh1Δ/Δ* suggested the induction of stress associated
148 phenotypes in the absence of environmental stressors. In contrast, the loss of *EDC3* did not
149 impair colony growth at 30°C and 37°C in SC5314 (Fig S2. A). Thus, we focused the remainder
150 of this study on *DHH1*.
151

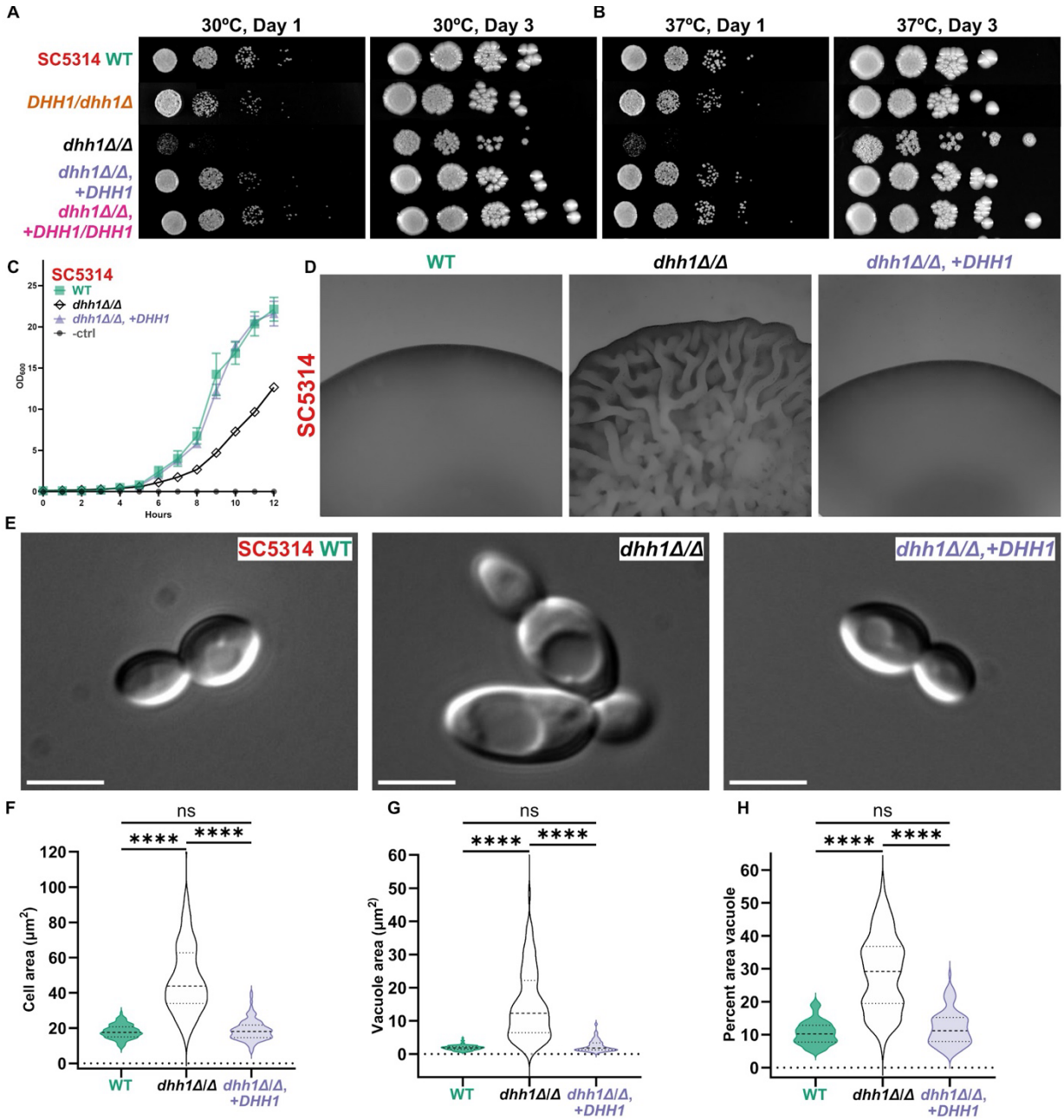

Figure 2. *DHH1* is required for WT growth and morphology in SC5314. A. and **B.** *dhh1Δ/Δ* resulted in slow growth at 30°C and 37°C on YPD plates, which was complemented by a single copy of *DHH1*. **C.** *dhh1Δ/Δ* had reduced growth in liquid YPD (30°C). WT and mutant strains were grown in triplicate. Impaired *dhh1Δ/Δ* exponential growth was rescued by complementation (*dhh1Δ/Δ*, *+DHH1*). Error bars show 95% CI. **D.** Colonies lacking *DHH1* have a wrinkled morphology (4 days, YPD agar, 37°C). 25X magnification. **E.** DIC images of exponentially growing cells (YPD, 30°C) show enlarged cell bodies and vacuoles in *dhh1Δ/Δ*. Scale bars = 5μm. **F.- H.** Quantification of cell and vacuolar enlargement in *dhh1Δ/Δ* (N = 100 cells per strain; ****P < 0.0001, Kruskal-Wallis tests).

152

153

DHH1 is necessary for SC5314 WT filamentation

We next examined filamentation in *dhh1Δ/Δ*. SC5314 *dhh1Δ/Δ* cells were larger than WT and complement strains after 4 hours of filamentation, with the cell body taking up a greater proportion of the total length (Fig 3. A). However, the median length to width ratio of *dhh1Δ/Δ* cells was significantly smaller, due to impaired germ tube elongation (Fig 3. B). After 16 hours of planktonic filamentation, *dhh1Δ/Δ* cells remained enlarged with thick curved germ tubes and fewer septa compared to WT and complement strains (Fig 3. C). The median length to width ratio of *dhh1Δ/Δ* at 16 hours was also significantly less than the other strains (Fig 3. D). In summary, we found that a single copy of *DHH1* sufficiently supported WT planktonic filamentation, while homozygous deletion resulted in abnormal planktonic filamentous growth.

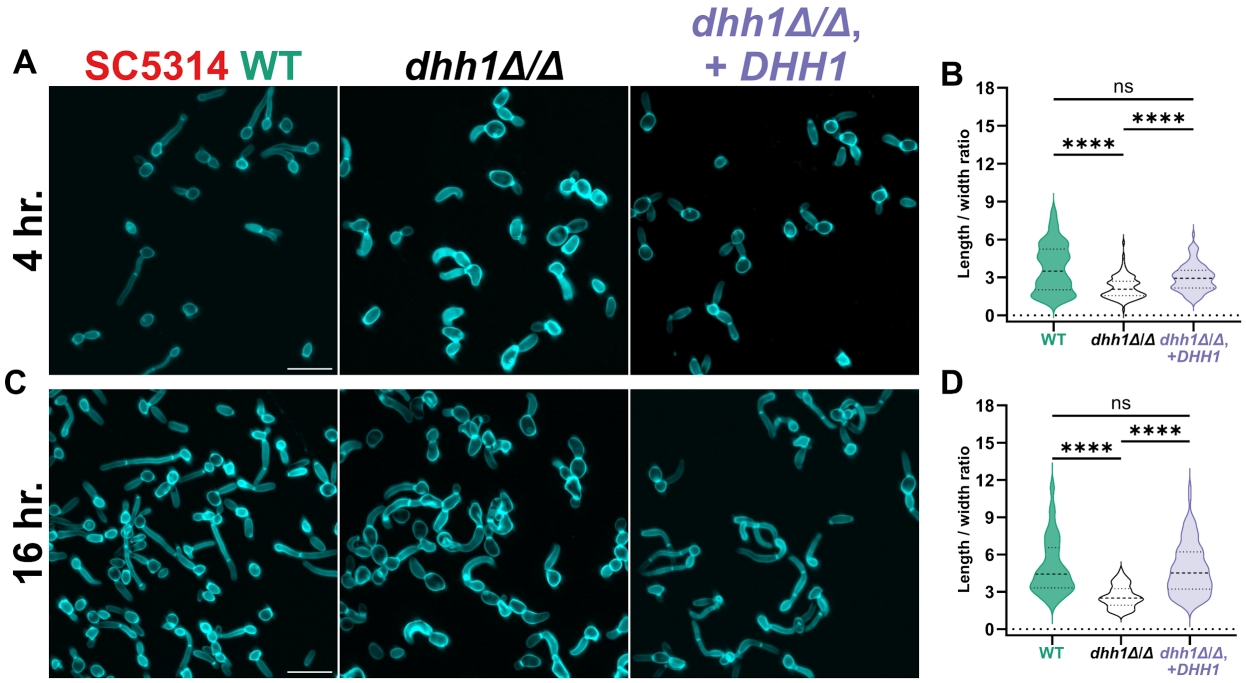

Figure 3. *DHH1* is required for wildtype planktonic filamentation. WT and mutant strains grown under physiologically relevant filamentation conditions (37°C, RPMI + 10% FBS). **A.** and **B.** After 4-hours of filamentation, *dhh1Δ/Δ* had reduced germ tube development defined by the median ratio of cell length to width. **C.** and **D.** After 16-hours of filamentation, *dhh1Δ/Δ* had less developed germ tubes with fewer septa compared to wildtype and complement strains. (Scale bars = 20μm; N = 100 cells, ****P < 0.0001, Kruskal-Wallis tests).

171 Due to the significant impairment of planktonic filamentation in SC5314 *dhh1Δ/Δ,* we expected
172 *dhh1Δ/Δ* to exhibit comparatively short defective biofilms. Surprisingly, *dhh1Δ/Δ* generated
173 deep, diffuse biofilms compared to WT and complement strains (Fig 4. A-B). Nevertheless,
174 *dhh1Δ/Δ* biofilms exhibited other key differences. In WT and *DHH1* complement strains, cells
175 were concentrated near the base of the biofilm (Fig 4. C). Using average pixel intensity as a
176 proxy for cell density, we quantified biofilm architecture, and found *dhh1Δ/Δ* biofilms were
177 altered with a maximum cell density further removed from the basal layer of the biofilm
178 compared to WT and *DHH1* complement (Fig 4. D). This modified biofilm structure may result
179 from the somewhat hyperfilamentous *dhh1Δ/Δ* strain, via decreased yeast cell proliferation at
180 the base of the structure.
181 Next, we surveyed the phenotype of colonies during invasive growth on spider media. After 6
182 days of growth at 37°C, *dhh1Δ/Δ* colonies revealed a wrinkled hyphal phenotype but a marked
183 absence of hyperfilamentous margins found in WT SC5314 (Fig 4. E). Compared to strains with
184 at least one copy of *DHH1*, *dhh1Δ/Δ* colonies grew more vertically with tighter wrinkles (Fig 4.
185 E). Again as in the other filamentation assays, our complement strain with a single *DHH1* copy
186 produced phenotypically WT colonies on spider media (Fig 4. E). Furthermore, in contrast to
187 *dhh1Δ/Δ, edc3Δ/Δ* was not filamentation impaired in all three filamentation assays (Fig S2. B-F).
188 In conclusion, SC5314 *dhh1Δ/Δ* failed to generate WT germ tubes, biofilm composition or
189 invasive colonies on spider media supporting a role for this RNA decay factor in filamentation.

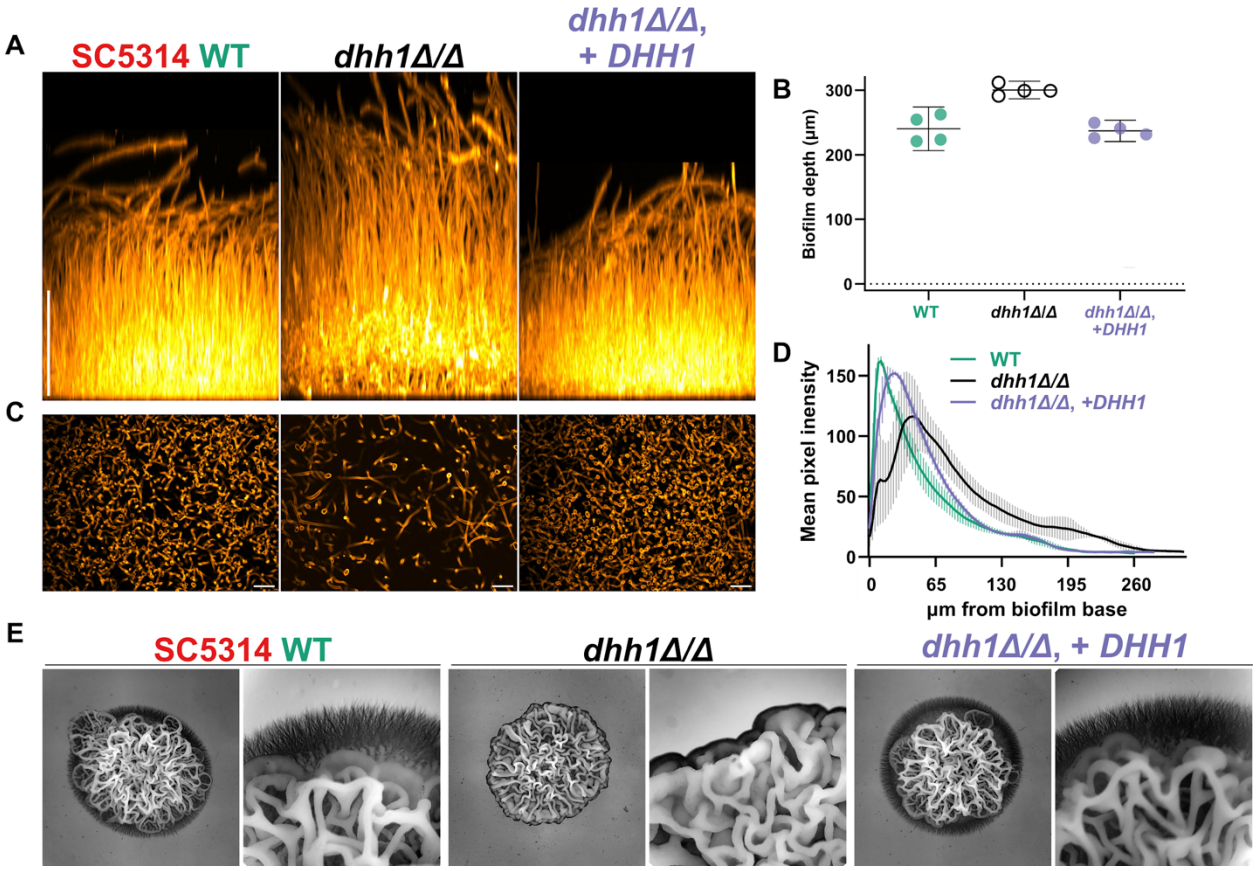

Figure 4. Absence of *DHH1* alters SC5314 biofilm and spider colony morphology. WT and mutant strains grown in two *in vitro* filamentation assays. **A.** and **B.** WT and mutant biofilms after a 24-hours (37°C, RPMI + 10% FBS) *dhh1Δ/Δ* has thicker biofilms. Scale bar = 100µm, 95% CI. **C.** Basal views 26µm from the bottom of the biofilm showed a reduced density of *dhh1Δ/Δ* cells. Scale bar = 20µm. **D.** Average pixel intensity (cell wall stain) from 4 replicate biofilms (SD) varied with biofilm depth. Strains with at least one copy of *DHH1* had a greater concentration of cells closer to the base of the biofilm than *dhh1Δ/Δ*. **E.** Colonies on spider plates require *DHH1* for hyperfilamentous margins (6 days, 37°C). 6X and 25X magnification.

Loss of DHH1 disrupts numerous pathways involved in metabolism and cellular morphology in SC5314

Given the severe phenotypic defects in SC5314 *dhh1Δ/Δ* yeast and hyphae, we next used RNA-seq to identify differentially expressed genes in yeast (30°C, YPD) and early hyphae (37°C, RPMI + 10% FBS, 4 hours) in triplicate (see methods for details) [60]. After removing poorly transcribed genes (Fig S8. A-B) we evaluated samples by PCA (Fig S9. A) and differential expression using DEseq2 [61]. In YPD, *dhh1Δ/Δ* yeast had 1,244 genes significantly downregulated and 1,408 genes significantly upregulated (Padj < 0.01) compared to wildtype (Fig 5. A, Table S1). Interestingly, *dhh1Δ/Δ* yeast upregulated multiple genes associated with

199 hyphae inducing stress, including *RHR2*, *ECE1*, and *HWP1* (Fig 5. A; Fig S3. C-D). Indeed, GO
200 terms corresponding to hyphal stress, such as hyphal cell wall and carbohydrate transport, were
201 enriched in upregulated genes (Fig 5. B). In RPMI, *dhh1Δ/Δ* hyphae had 1,151 genes
202 downregulated and 1,269 genes upregulated (Padj < 0.01) (Fig 5. C, Table S2). Lactate and
203 sugar transport genes were upregulated in *dhh1Δ/Δ* RPMI including *JEN1* and *HGT12* (Fig 5.
204 C). Under these conditions, *dhh1Δ/Δ* inappropriately expressed many cell wall-associated
205 transcripts. Hyphal adhesin *ALS1* was downregulated while yeast cell wall protein *YWP1* was
206 upregulated (Fig 5. C; Fig S3. E). Genes upregulated in *dhh1Δ/Δ* hyphae were enriched in GO
207 terms related to transport, metabolism, and ergosterol biosynthesis (Fig 5. D). While most
208 changes in expression were specific to environmental conditions, there was significant overlap
209 in the genes affected by *dhh1Δ/Δ* during growth in YPD and RPMI (Hypergeometric test, P <
210 $2.3e^{-22}$; Fig 5. E). Transcription factors regulating cell morphology were also differentially
211 expressed *dhh1Δ/Δ* in both conditions (Fig 5. F). Interestingly, while most TFs shifted in the
212 same direction in both conditions, hyphal repressor *NRG1* [62, 63] and cell cycle/cell wall stress
213 regulator *SWI6* [64, 65] were downregulated in YPD but upregulated in RPMI (Fig 5. F). In
214 summary, RNA-seq established widespread gene expression aberrations in SC5314 *dhh1Δ/Δ*
215 yeast and hyphae.

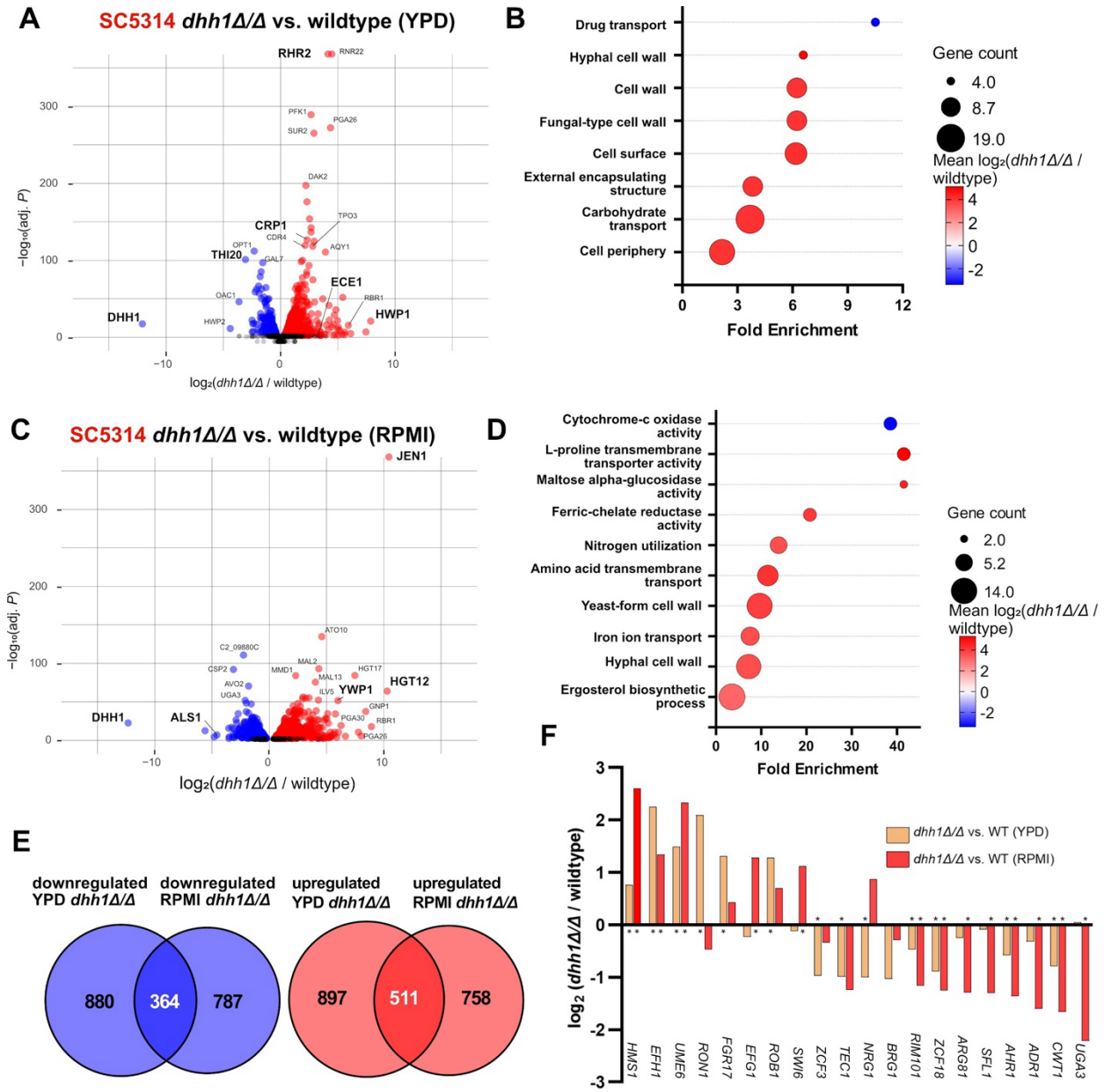

Figure 5. RNA-seq exposed differential gene expression in SC5314 *dhh1Δ/Δ* grown in YPD and RPMI. A. Volcano plot depicts genes are significantly up (red) and down (blue) -regulated in *dhh1Δ/Δ* yeast-form growth compared to wildtype (Padj < 0.01). Genes associated with filamentation stress were prominently upregulated (Table S1). **B.** GO terms enriched in *dhh1Δ/Δ* YPD include transport and cell wall terms (Padj < 0.1). **C.** Volcano plot depicts gene expression differences in *dhh1Δ/Δ* vs wildtype during early hyphal growth (Table S2, Padj < 0.01). Genes associated with metabolite transport and the yeast/hyphal cell wall were differentially expressed in *dhh1Δ/Δ*. **D.** GO terms enriched in *dhh1Δ/Δ* RPMI include transport, cell wall, and metabolic terms (Padj < 0.1). **E.** A significant number of *dhh1Δ/Δ* transcripts were downregulated ($P = 2.28e^{-22}$), and upregulated ($P = 4.37e^{-52}$), respectively, in both YPD and RPMI conditions (Hypergeometric tests). However, most differentially expressed genes were environmentally specific. **F.** Differential expression of transcription factors regulating morphogenesis in *dhh1Δ/Δ* in YPD and RPMI (* indicates Padj < 0.01; DEseq2).

216

217

218 **Filamentation dependent transcriptome remodeling is reduced in *dhh1Δ/Δ***

219 We next investigated the role of *DHH1* in gene regulation during filamentation. Comparing RNA-
220 seq results from WT SC5314 grown in RPMI and YPD showed the known extensive
221 transcriptome remodeling that occurs during filamentation, with 2,488 downregulated and 2,496
222 upregulated genes (Fig 6. A, Table S3). Hyphal cell wall proteins and ubiquitination factors such
223 as *HWP1* and *BUL1* were upregulated in WT RPMI compared to WT YPD (Fig 6. A). GO terms
224 related to ribosomal RNA, ribosomal proteins, and translation elongation were all enriched in
225 genes downregulated in WT hyphae, strongly indicating a general reduction in mRNA
226 translation (Fig 6. B). The majority of upregulated GO terms in WT RPMI were enriched in
227 carbohydrate transporters responding to the shift from rich YPD to carbohydrate poor RPMI (Fig
228 6. C). These results are consistent with known transcriptional changes that occur during WT
229 filamentation [13, 66–72].

230 We hypothesized that impaired mRNA decay in *dhh1Δ/Δ* would blunt the downregulation of a
231 subset of genes during filamentation. Indeed, transcriptional remodeling of *dhh1Δ/Δ* was
232 reduced with 1,795 downregulated and 1,919 upregulated genes, only 75% of the total number
233 of genes remodeled in WT (Fig 6. D). Genes uniquely differentially expressed in WT
234 filamentation were related to metabolism and transmembrane transport (downregulated) and
235 nucleic acid decay (upregulated). The number of up and downregulated genes during WT
236 filamentation was almost equal with only 8 more genes upregulated compared to downregulated
237 (Fig 6. A). However, *dhh1Δ/Δ* had 124 fewer genes downregulated compared to upregulated,
238 possibly due to impaired mRNA degradation (Fig 6. D). Most of the GO terms enriched in
239 downregulated genes in filamenting *dhh1Δ/Δ* were the same as WT (cf. Fig 6. B & E). Similarly,
240 most of the GO terms enriched in upregulated genes in filamenting *dhh1Δ/Δ* were also enriched
241 in filamenting WT cells (cf. Fig 6. C & F). Uniquely, terms related to lipid catabolism were
242 upregulated in *dhh1Δ/Δ* but not WT (cf. Fig 6. C & F). Changes in the expression of
243 morphology-related transcription factors were generally less pronounced in *dhh1Δ/Δ* than WT.

For some genes this was due to increased basal expression in YPD (Fig 5. F, Fig 6. G). Interestingly, unlike in WT, the filamentation repressor gene *NRG1* was not significantly downregulated in filamenting *dhh1Δ/Δ*, suggesting a mechanism for continued repression of select hyphal genes (Fig 6. G). The vast majority of differentially expressed genes in filamenting *dhh1Δ/Δ* were a subset of WT remodeling (Hypergeometric test, P = 0; Fig 6. H). In general,

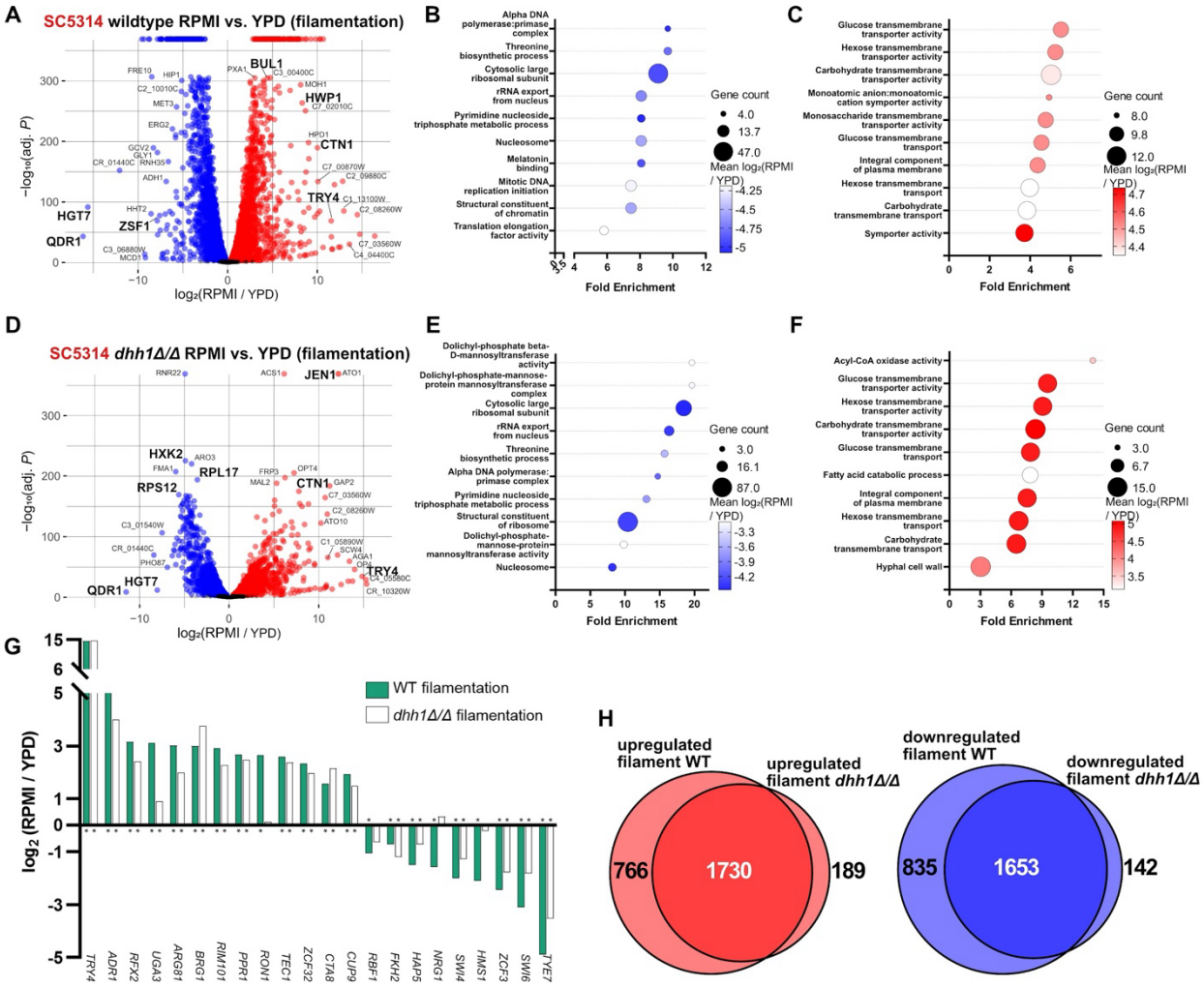

Figure 6. RNA-seq reveals transcriptome differences between SC5314 wildtype and *dhh1Δ/Δ* during filamentation. A. Volcano plots comparing the transcriptomes of WT SC5314 grown in YPD and RPMI demonstrate extensive remodeling during filamentation (Table S3, Padj < 0.01). **B.** Expected GO terms were downregulated, and **C.** upregulated during WT filamentation (Padj < 0.1). **D.** Comparing the transcriptomes of *dhh1Δ/Δ* grown in YPD and RPMI showed impaired remodeling during filamentation (Table S4, Padj < 0.01). **E.** Similar GO terms were downregulated, and **F.** upregulated in filamenting *dhh1Δ/Δ* and WT (Padj < 0.1). Unlike wildtype, *dhh1Δ/Δ* upregulated terms related to lipid catabolism during filamentation. **G.** Transcription factors regulating morphogenesis had blunted remodeling in *dhh1Δ/Δ*. (* indicates Padj < 0.01; DEseq2). **H.** Most genes differentially expressed during *dhh1Δ/Δ* filamentation are subsets of the WT remodeling response. A significant number of genes were downregulated or upregulated in both filamenting *dhh1Δ/Δ* and wild type (Hypergeometric tests, P = 0).

249 SC5314 *dhh1Δ/Δ* had a more modest transcriptome remodeling response during filamentation
250 than WT.

251 **Absence of *DHH1* alters growth, heat tolerance, and filamentation in diverse**
252 **strains**

253 Recent studies have identified considerable heterogeneity in regulatory networks that control
254 filamentation in diverse *C. albicans* strains [14, 73]. We next investigated the morphological
255 impacts of *DHH1* deletion in four additional strains representing the major *C. albicans* clades
256 [58]. In all backgrounds, we found *dhh1Δ/Δ* impaired YPD colony growth at both 30°C and
257 37°C, and only a single copy of *DHH1* was necessary for a WT appearance (Fig 7. A).
258 Interestingly, the extent of *dhh1Δ/Δ* growth reduction varied with the background strain. For
259 example, P75010 *dhh1Δ/Δ* colonies appeared similar in size to WT by Day 3, while P76067 and
260 P57055 *dhh1Δ/Δ* colonies were growth impaired across all temperatures and time points (Fig 7.
261 A). A similar trend was observed in liquid YPD, with P75010 exhibiting a relatively modest
262 decrease in growth (Fig 7. B). While none of the other *dhh1Δ/Δ* strains phenocopied the
263 extensive wrinkled morphology of SC5314 *dhh1Δ/Δ* grown at 37°C on YPD plates (Fig 2. D),
264 they each diverged from WT with distinct texture in the center of the colony (Fig 7. C). In the
265 absence of *DHH1,* hyperfilamentous backgrounds (P76067, P87) lost their distinct invasive
266 margins on spider media (Fig 7. D), while less filamentous strains (P75010, P57055) produced
267 *dhh1Δ/Δ* colonies with wrinkling reminiscent of SC5314 *dhh1Δ/Δ* (Fig 4. E, Fig 7. D). Thus, as in
268 SC5314, loss of *DHH1* in four diverse *C. albicans* strains reduced yeast growth, altered colony
269 morphology under heat stress, and produced phenotypically non-WT colonies on spider media.
270 These data support a central role in growth and filamentation for the RNA decay factor Dhh1
271 across *C. albicans* strain backgrounds.

272

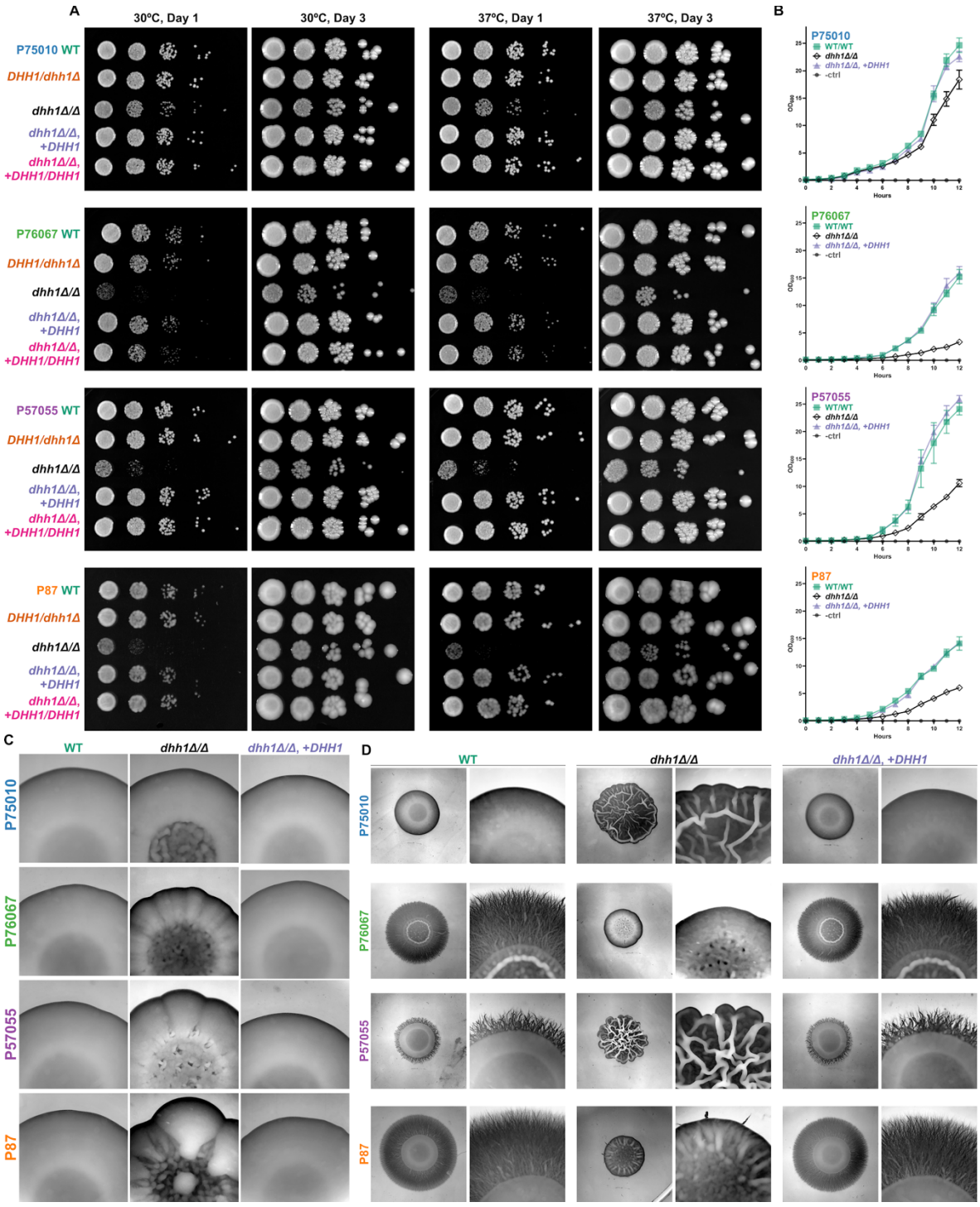

Figure 7. *DHH1* is required for wildtype growth and colony morphology in diverse strains. As in SC5314, DHH1 is required for wildtype growth, heat tolerance, and filamentation on spider media. Additionally, *dhh1Δ/Δ* impaired growth to a greater extent in hyperfilamentous strains. **A.** *dhh1Δ/Δ* resulted in slow colony growth at 30°C and 37°C on YPD plates, the extent of which varied with background strain. **B.** *dhh1Δ/Δ* reduced growth in liquid YPD (30°C). WT and mutant strains were grown in triplicate. Impairment of *dhh1Δ/Δ* exponential growth varied with strain and was rescued by complementation (*dhh1Δ/Δ*, +*DHH1*). Error bars show CI = 95%. **C.** Colonies lacking *DHH1* have a non-WT textured morphology during mild heat stress (4 days, YPD agar, 37°C). 25X magnification. **D.** Spider colony morphology varies between strains and requires *DHH1* for WT phenotype (6 days, 37°C). 6X and 25X magnification.

274 **SC5314 and P57055 transcriptomes exhibit analogous responses to *DHH1***
275 **deletion**

276 Our RNA-seq results indicated that *dhh1Δ/Δ* disrupts the expression of a wide variety of genes
277 and blunts the induction of the hyphal gene regulatory program in SC5314. To validate these
278 effects and identify genes whose expression is impacted by *dhh1Δ/Δ* in other genetic
279 backgrounds, we next used RNA-seq to identify differentially expressed genes in P57055 yeast
280 (30°C, YPD) and early hyphae (37°C, RPMI + 10% FBS, 4 hours) in triplicate (see methods for
281 details). As in SC3514, loss of *DHH1* in P57055 extensively altered the transcriptome in both
282 yeast and hyphae (Fig. S4, Table S5-S6) as well as during filamentation (Fig. S5, Table S7-S8).
283 Comparison of the RNA-seq data from SC5314 and P57055 grown in YPD, revealed a core of
284 down (457) and upregulated (632) genes in *dhh1Δ/Δ* strains compared to their respective
285 wildtype (Fig 8. A, Table S12). Strikingly, this core set was enriched with GO terms relating to
286 catabolism, metabolism, and hyphal cell wall (Fig 8. B-C). The effects of Dhh1 deletion on gene
287 expression were more similar during growth in RPMI, with 883 genes down and 901 genes
288 upregulated in both deletion strains (Fig 8. D, Table S13). Genes downregulated in both deletion
289 strains were enriched for GO terms relating to transcription, transport, and zinc binding (Fig 8.
290 E), while metabolic terms and yeast-form cell wall were enriched in genes upregulated (Fig 8. F)
291 in both *dhh1Δ/Δ* strains grown in RPMI. Interestingly, morphology related TFs were differentially
292 expressed in both *dhh1Δ/Δ* strains (Fig 5. F, Fig S4. F). For example the hyphal repressor
293 *NRG1* was significantly downregulated in YPD *dhh1Δ/Δ* SC5314 (Padj = 0) and P57055 (Padj =
294 $3.96e^{-15}$) (Table S1, S5). While regulators of hyphal growth *EFH1* and *UME6* were upregulated
295 in both *dhh1Δ/Δ* strains in YPD and RPMI (Fig 5. F, Fig S4. F). These results define a core set
296 of genes and pathways dependent on Dhh1 in divergent *C. albicans* strains (Table S12-S13).

297 Finally, we examined the impact of *dhh1Δ/Δ* on filamentation in SC5314 and P57055. In
298 wildtype strains, transcriptome remodeling was highly correlated (2,085 genes downregulated

299 and 2,084 genes upregulated) (Fig 8. G) and largely involved known transcriptional changes
300 that occur during filamentation (Fig 8. H-I) [13, 66–72]. In comparison, the transcriptional
301 response to filamentation in the two *dhh1Δ/Δ* strains was somewhat less consistent with 1,375
302 genes downregulated and 1,268 genes upregulated (Fig 8. J). As in filamenting SC5314
303 *dhh1Δ/Δ* alone (Fig 6. B-C, E-F), the majority of the overlapping enriched GO terms in
304 filamenting *dhh1Δ/Δ* SC5314 and P57055 (Fig 8. K-L) were a subset of the WT terms (Fig 8. H-
305 I). In both filamenting *dhh1Δ/Δ* strains, the expression of morphology-related transcription
306 factors was blunted compared to WT (Fig 6. G, Fig S5. G). Notably, genes downregulated in
307 both *dhh1Δ/Δ* deletion strains were enriched in hyphal cell wall functions (Fig 8. K), suggesting
308 a common defect in appropriate induction of hyphal wall programs during filamentation.
309 Together, these results indicate that loss of *DHH1* causes consistent defects in the
310 morphological transition between yeast and hyphal growth in two diverse clinical isolates of *C.*
311 *albicans* (Fig 9. A-B).

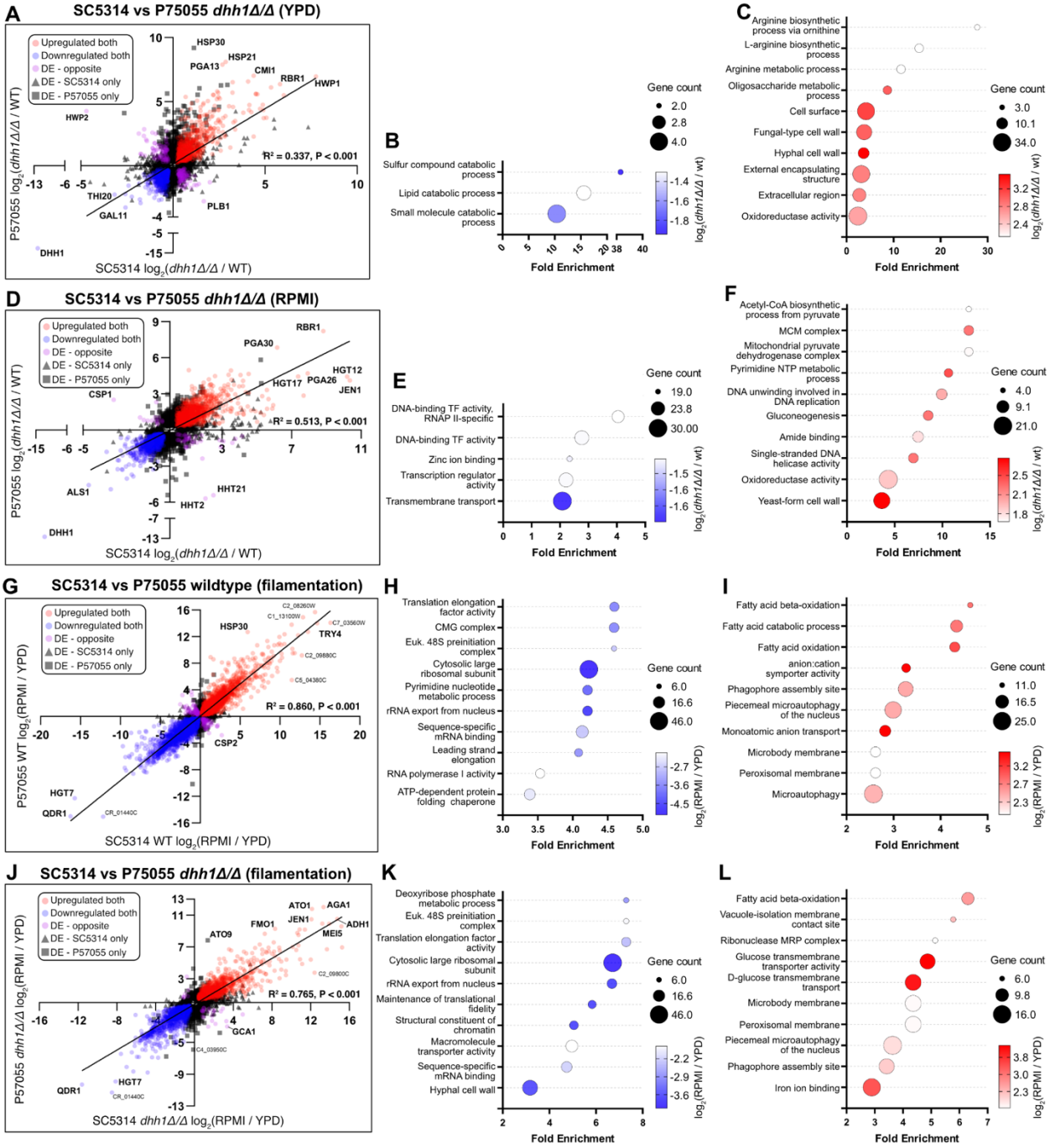

Figure 8. Differentially expressed genes and GO terms in *dhh1Δ/Δ* and WT strains correlated between SC5314 and P57055. A. Scatter plot of DE genes (Padj < 0.01) in both SC5314 *dhh1Δ/Δ* and P57055 *dhh1Δ/Δ* in YPD is moderately correlated. GO analysis of core genes **B.** down and **C.** upregulated in both *dhh1Δ/Δ* strains in YPD, emphasize terms related to the cell wall and biosynthesis. **D.** Scatter plot of DE genes (Padj < 0.01) in both SC5314 *dhh1Δ/Δ* and P57055 *dhh1Δ/Δ* in RPMI has a greater correlation than in YPD reflecting a common stress response. GO analysis of core genes **E.** downregulated and **F.** upregulated in both *dhh1Δ/Δ* strains in RPMI. **G.** Scatter plot of DE genes in both WT SC5314 and WT P57055 during filamentation (Padj < 0.01) is highly correlated. GO analysis of core genes **H.** down and **I.** upregulated during SC5314 and P57055 WT filamentation shows expected regulatory changes. **J.** Scatter plot of DE genes in SC5314 *dhh1Δ/Δ* and P57055 *dhh1Δ/Δ* during filamentation are still correlated (Padj < 0.01). GO analysis of core genes **K.** down and **L**. upregulated are generally a subset of WT except for downregulation of hyphal wall genes.

312

313 ## Discussion

314 Foundational research on the genetic bases of filamentation largely focused on transcription
315 factors [9] such as *BRG1* [74], *UME6* [75], and *EFG1* [12]. More recently, growing evidence for
316 post-transcriptional regulation of filamentation has added an additional layer of control [15, 16,
317 22]. Previous studies reported that loss of a single *DHH1* copy impairs filamentation [35] and the
318 requirement of *EDC3* for WT stress tolerance and filamentation [36, 37]. These results
319 suggested PB factors have different functions in *C. albicans* as compared to their homologs in
320 *S. cerevisiae* and *S. pombe* [35, 43, 56, 76, 77]. However, the molecular methods originally
321 used to generate *C. albicans DHH1/dhh1Δ* and *edc3Δ/Δ* can lead to confounding effects that
322 require complementation controls [78–80]. Unlike *S. cerevisiae* [46, 48, 81], the gene regulatory
323 effects of *DHH1* deletion, both during yeast and hyphal growth, were not previously
324 characterized in *C. albicans*. Here we investigated the roles of PB factors Dhh1 and Edc3 in *C.*
325 *albicans* growth, filamentation, and gene expression across multiple strains.
326 Our work helps refine our understanding of Dhh1 and Edc3 in PB formation. Previous studies
327 reported Edc3 was necessary for observable PBs during *C. albicans* glucose starvation [36].
328 Contrary to this, *S. cerevisiae* PBs condense in the absence of many individual protein factors,
329 including Dhh1 and Edc3 [44]. Our findings align with the roles of these genes in *S. cerevisiae*
330 and other eukaryotes. In *C. albicans*, PBs condense during heat shock without Dhh1 or Edc3
331 (Fig 1. F-G, Fig S1. B-C). Our results suggest that, as in *S. cerevisiae* [27, 44, 82], the absence
332 of multiple scaffolding proteins would be required to completely disassemble *C. albicans* P-
333 bodies [27, 44, 82]. Additionally, we found Dhh1 was both present in PBs and cytoplasmically
334 diffuse, suggesting a PB-independent function in the cytoplasm (Fig 1. B), as in *S. cerevisiae*
335 [44, 45]. For example, in *S. cerevisiae*, impaired ATPase activity of Dhh1 caused it to
336 accumulate in PBs and impaired mRNA decay of specific transcripts possibly due to decreased

concentration in the cytoplasm [25, 45]. Thus, *C. albicans* PBs may share many of the well documented functions and characteristics of their homologous condensates from *S. cerevisiae*.

Our phenotypic results differ from previous work. First, haploinsufficiency in filamentation was previously reported for *DHH1/dhh1Δ* in BWP17 [35]. In contrast, we found that only homozygous *dhh1Δ/Δ* mutations had aberrant filamentation in five diverse *C. albicans* strains (Fig. 3-4, 7D). Additionally, a single copy of *DHH1* complements these growth defects (Fig. 3-4, 7D). This suggests *DHH1* is not a rate limiting factor for mRNA decay. Additionally, we found that *EDC3* is not required for heat tolerance or filamentation in five different strains, contrary to results from BWP17 [36, 37] (Fig. S2). While *EDC3* may not be essential for filamentation, retaining this gene likely confers an as of yet unknown evolutionary advantage to *C. albicans*. For example, Edc3 contributes to suppressing the misexpression of starvation genes in *S. cerevisiae* [54]. Although we found different phenotypes for deletion of *DHH1* and *EDC3* than in prior studies, this earlier work used a deletion approach that can cause off-target effects [78–80] and complementation studies confirming the deletions were not performed [35, 36, 83]. Our results highlight the power of targeted deletion through CRISPR-Cas9 and the importance of complementation analysis of genetic phenotypes.

Recently, a number of studies have reported considerable heterogeneity in the phenotypes of diverse *C. albicans* strains, which can vary depending on environmental conditions [58, 84, 85]. Comparison of phenotypes across diverse strains has also been used to identify core functions of genes [14, 73]. We used this strategy to compare the functions of Dhh1 in filamentation in SC5314 and four additional strains. After growing diverse *dhh1Δ/Δ* strains on spider media, we found deletions in hyperfilamentous strains produced colonies that failed to invade agar, yet presented other aspects of hyphal morphology (Fig 4. E, Fig 7. D). Interestingly, in strains with minimal filamentation potential (P75010 and P57055), *dhh1Δ/Δ* presented colonies with more pronounced wrinkling (Fig 7. D). Furthermore, *dhh1Δ/Δ* in non-filamentous P75010 had a

362 minimal reduction in yeast-form growth rates as compared to highly filamentous strains like
363 P76067 (Fig 7. A-B). One intriguing possibility is that highly filamentous strains are more reliant
364 on mRNA decay to prevent the inappropriate expression of stress response and filamentation
365 genes (Fig 9A). In conclusion, *dhh1Δ/Δ* impacts growth and colony morphology in multiple
366 backgrounds in a manner correlated with their intrinsic filamentation propensity.

367 We also investigated the effects of *dhh1Δ/Δ* on the transcriptomes of *C. albicans* under both
368 yeast and filamentous growth. Strikingly, we found the absence of *DHH1* induces major
369 transcriptomic changes in both yeast (YPD) and hyphae (RPMI) in SC5314 and P57055 (Fig. 5,
370 Fig. S4). These changes suggest an "identity crisis", such that the deletion strains express
371 hyphal genes under yeast-growth conditions (Fig 9. B). In YPD, *dhh1Δ/Δ* upregulates genes
372 normally associated with hyphal virulence such as *RHR2* [86], *ECE1* [5], and *HWP1* [87] in
373 SC5314 and P57055 (Figs 5. A, S3 C-D, S4 A; Tables S1 & S5). However, *ECE1* and *RHR2*
374 upregulation is more modest in *dhh1Δ/Δ* P57055 and only approaches statistical significance
375 (Padj = 0.076 and 0.013), respectively. (Table S1, Table S5). Under both yeast and hyphal
376 conditions, genes upregulated by *dhh1Δ/Δ* are enriched in cell wall and cell surface GO terms in
377 both SC5314 and P57055 (Fig. 5-6, Fig. S4-S5). The resulting effect is expression of cell wall
378 genes that are unsuitable to the growth condition (Fig 9B). For example, in both strains *dhh1Δ/Δ*
379 upregulates yeast cell wall protein *YWP1* and downregulates hyphal adhesion *ALS1* in RPMI
380 (Figs 5 C, S3 E, S4 C; Tables S2 & S6). These results support a model in which Dhh1 prevents
381 the misexpression of genes involved in the transition between yeast and hyphal growth.

382 A number of transcription factors are known to regulate filamentation [9, 68, 75]. Our results
383 show that DHH1 deletion led to inappropriate expression of several key transcriptional
384 regulators in both SC5314 and P57055 (Fig 5. F, Fig S4. F). Hyphal repressor *NRG1* [62, 63]
385 was downregulated in YPD, potentially de-repressing downstream hyphal associated genes
386 across both *dhh1Δ/Δ* strains (Fig 5. F, Table S1, S5). Similarly, regulators of hyphal growth

387 *EFH1* and *UME6* were upregulated in both *dhh1Δ/Δ* strains in YPD and RPMI (Fig 5. F, Fig S4.
388 F). We find the upregulation of *UME6* particularly interesting because *UME6* constitutive
389 expression produces hyphae under non-filament inducing conditions [75]. Furthermore, *UME6*
390 has an extremely long 5' UTR mediating translational efficiency, and it has been proposed that
391 sequences in the *UME6* 5' UTR could direct its transcripts to PBs [88]. The misregulation of
392 these transcription factors could directly upregulate hyphal cell wall genes and contribute to the
393 textured phenotype seen in all our *dhh1Δ/Δ* strains at 37°C (Fig 2. D, Fig 7. C). Interestingly,
394 under filamentation conditions SC5314 and P57055 *dhh1Δ/Δ* strains upregulated select hyphal
395 transcription factors (e.g. *UME6*, *SWI6*) more than their respective WT strains (Fig 5. F, Fig S4.
396 F). We propose that loss of *DHH1* leads to pleiotropic hyphal morphology through alterations in
397 the expression of hyphal transcription factors and their downstream regulatory networks (Figs 7
398 D & S4 F).

399 In many species stochastic transcriptional noise serves as a form of "bet-hedging" for acute
400 environmental stressors [38–40]. For example, within a population of *C. albicans*, individual cells
401 heterogeneously express the hyphal transcription factor Efg1, adapting colonization to host
402 immune status [89]. Our data support a model where *C. albicans* adapts to diverse host
403 microenvironments by transcribing multiple stress-associated genes, while simultaneously
404 buffering expression via mRNA decay. This strategy promotes rapid responses to diverse
405 stressors without investing energy towards environmentally inappropriate proteomic and
406 phenotypic remodeling. Consistent with this model, we find blunted transcriptome remodeling
407 during filamentation in both *dhh1Δ/Δ* strains as compared to their respective wildtype strains
408 (Fig 6. A, D, Fig S5. A, D). We postulate this results from upregulation of stress-response genes
409 in YPD and defective mRNA decay in the absence of *DHH1*. Further work is needed to test this
410 model of decay-mediated suppression of noisy stress-response genes in *C. albicans* as a
411 mechanism to regulate appropriate environmental adaptation.

A

Strain	WT spider filamentation	*dhh1Δ/Δ* yeast-form growth	*dhh1Δ/Δ* colony morphology at 37°C	*dhh1Δ/Δ* spider filamentation
P76067	+ + + +	- - - -	+ +	- - - -
P87	+ + + +	- - - -	+ + +	- - - -
SC5314	+ + +	- -	+ + + +	- - -
P57055	+ +	- - -	+ +	- -
P75010	-	-	+	+

B

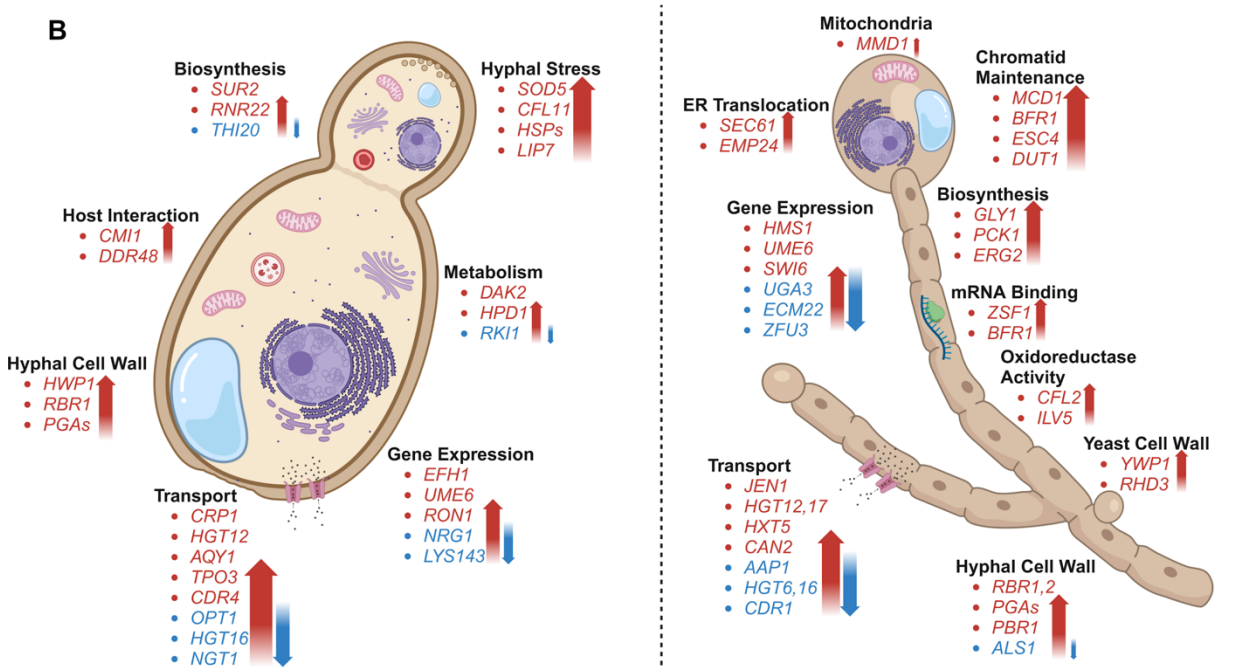

Figure 9. Phenotypic and transcriptomic outcomes in diverse *dhh1Δ/Δ* strains. Despite differences between WT background strains, loss of *DHH1* is associated with specific morphological and transcriptomic outcomes across diverse clades. **A**. Hyperfilamentous strains are more phenotypically sensitive to the loss of *DHH1*. **B.** Diagram of overlapping transcripts and terms in SC5314 *dhh1Δ/Δ* and P57055 *dhh1Δ/Δ* in YPD and RPMI. Under yeast-form growth conditions *dhh1Δ/Δ* fails to repress the hyphal stress response. Under hyphal growth conditions *dhh1Δ/Δ* presents a misregulated transcriptome including persistence of yeast features. Genes in red were significantly upregulated, while genes in blue were significantly downregulated (Padj < 0.01).

412 As with our phenotype results, our transcriptome analysis of *C. albicans DHH1* deletion strains
413 suggests a similar regulatory role as its homologs in other fungi. For example, in *C. neoformans*,
414 the Dhh1 homologue Vad1 is required for virulence and suppresses the transcript of mating
415 pheromone *MFα* under vegetative conditions [51, 90, 91]. This suggests Dhh1/Vad1-mediated
416 RNA decay for environmentally suitable gene expression. In *S. cerevisiae*, Dhh1 has been
417 reported to repress genes associated with nutrient limitation under optimal growth conditions
418 [48]. Additionally, it has been proposed that transcripts with slow translation and poor codon
419 optimality are targeted for Dhh1 dependent mRNA decay [46, 47]. Our results suggest rare

420 codons do not mark genes for Dhh1-mediated mRNA decay in *C. albicans,* as genes
421 upregulated in SC5314 and P57055 *dhh1Δ/Δ* had higher codon adaptation index (CAI) values
422 than downregulated genes (Fig. S6). However, we found both *C. albicans dhh1Δ/Δ* strains
423 upregulate genes involved in cell wall and non-preferred carbon/nitrogen metabolism –
424 pathways similar to those that were de-repressed in *S. cerevisiae dhh1Δ* [48]. Thus, our results
425 are consistent with the observation that Dhh1 suppresses genes associated with nutrient
426 limitation in *S. cerevisiae.* We hypothesize that *C. albicans* Dhh1 and its homologues in other
427 fungi support environmentally optimal gene expression by buffering noisy transcription through
428 mRNA decay.

429 Altogether, our work identifies an important role for Dhh1 in regulating filamentation in *C.*
430 *albicans* and implicates post-transcriptional regulation in the control of key regulators of hyphal
431 growth. Future studies are needed to elucidate the features of transcripts repressed by Dhh1 in
432 *C. albicans* under different growth conditions. For example, 4-thioU pulse-chase experiments
433 could identify changes in RNA stability in the *dhh1Δ/Δ* mutant to further investigate if Dhh1
434 promotes decay of noisy stress-response transcripts. Additionally, an auxin inducible
435 degradation system [92] knocking down Dhh1, could distinguish direct targets of Dhh1 mediated
436 decay from downstream stress-responses to dysregulated RNA metabolism. Regardless of the
437 outcomes of such studies, our work clearly defines an important role for Dhh1 in regulating
438 filamentous growth and gene expression in *C. albicans*.

439 Materials and methods

440 Strains and media

441 All strains (Table S9) were maintained as 15% glycerol stocks stored at -80°C. Before all
442 experiments, strains were streaked on YPD agar (MP Biomedicals) and grown for two days at
443 30°C. Single colonies were picked and grown in liquid YPD (2% Bacto Peptone, 2% dextrose,

444 1% yeast extract) on a rotator overnight at 30°C. For PB imaging in live yeast (Fig. 1 A-C, F-G
445 and Fig. S1 A-C), we used complete media (CM) (0.68% yeast nitrogenous base, 0.079% CSM
446 complete AA mixture, 2% dextrose) to minimize background fluorescence. The growth media for
447 planktonic filamentation and biofilm assays was RPMI 1640 (Gibco, minus phenol red) with 10%
448 FBS (Gibco). For PB (Edc3-mNeonGreen) imaging during filamentation (Fig. 1 E), we used
449 100% RPMI without phenol red due to background fluorescence of FBS. We evaluated
450 filamentous colony morphology with spider plates [93] (1% nutrient broth, 1% D-mannitol, 0.2%
451 K_2HPO_4, 2% agar).

452 **Strain construction**

453 WT strains and plasmids pV1093 and pRS316 were used for CRISPR-Cas9 genome editing
454 [57, 94]. mNeonGreen [95] was appended to the C-terminus of *EDC3* using lithium acetate
455 transformation and the SAT1 FLP/FRT cassette (pRS316) [94] without the CRISPR-Cas9
456 system. For all other gene insertions (including *DHH1*-mScarlet (Fig S7. A)) and our whole-gene
457 deletions, we used transient CRISPR-Cas9 [57] with the SAT1 FLP/FRT cassette [94] which
458 leaves a 34bp FRT scar in the genome. Optimal Cas9 guide RNAs and PAM sites were
459 selected from a database of unique sites [96]. The SAT1 FLP/FRT cassettes with C-terminal
460 *EDC3*mNeonGreen and *DHH1*mScarlet tags included sequences homologous to the 3' end of
461 the target genes and a GGSG linker [95]. To completely delete *EDC3* and *DHH1*, our cassettes
462 used homologous sequences upstream and downstream of the CDS (Fig S7. B). Additionally,
463 for the *DHH1* complement (*dhh1Δ/Δ* background) we inserted *DHH1* fused to the *TPI1* promoter
464 at the *MDR1* locus replacing the entire gene (Fig S7. C).

465 For plasmid transformations, single colonies were picked from 2 day YPD plates and incubated
466 in 5mL YPD on a rotator overnight at 30°C. The next day, the overnight culture was diluted to
467 OD_{600} = 0.2 in 50mL YPD and grown to OD_{600} = 0.8 (30°C, 300 RPM). Cells were collected by
468 centrifugation (1,600 RCF, 5 minutes) in a 50mL falcon tube, washed with 5mL sterile dH_2O,

469 resuspended 500µL LATE solution (0.1M LiAc/TE) and transferred to a 1.5mL microcentrifuge
470 tube. 1µg of each PCR product (sgRNA, caCas9, SAT1 FLP/FRT) and 10µL boiled calf thymus
471 DNA were added and cells were rotated for 30 minutes at 30°C before adding 700µL freshly
472 made PLATE solution (800µL 50% PEG 4,000, 100µL 10X TE, 100µL 1M LiAC). Cells were
473 then rotated overnight at 30°C. The next day, cells were gently mixed and incubated at 44°C for
474 15 minutes. The cells were harvested by centrifugation (1,500 RCF, 30 seconds), washed and
475 resuspended in 2mL YPD. Cells were then incubated for 5 hours at 30°C on the rotator in 15 mL
476 falcon tubes. After this recovery period, cells were harvested by centrifugation (1,600 RCF, 3
477 minutes and resuspended in 200µL YPD. 100µL of resuspended cells were plated on each of
478 two YPD plates with 400µg/mL nourseothricin (clonNAT/NTC; Goldbio #N-500-1) and incubated
479 at 30°C for 48 hours. We extracted gDNA [57, 97] and verified insertion of SAT1 FLP/FRT and
480 homo/heterozygosity in colonies by PCR.

481 Transformed colonies were incubated in a 15mL falcon tube with 10mL YPM (2% Bacto
482 Peptone, 2% maltose, 1% yeast extract) overnight to induce excision of the SAT1 FLP/FRT
483 cassette. Overnight YPM cultures were serially diluted by $1:10^5$ to $1:10^6$ and 100µL was spread
484 on YPD + 40µg/mL clonNAT plates and incubated at 30°C. After 48 hours, small colonies were
485 selected, indicative of SAT1 FLP excision. All strains were validated by gDNA PCR for cassette
486 insertion, homo/heterozygosity, and excision of SAT1 [57, 97]. We used *TDH3* as the control for
487 gDNA extraction and amplification. All strains, plasmids, guide RNA and PAM sites as well as
488 primers for strain construction and verification are listed in Table S9.

489 **Phenotype assays**

490 For PB imaging in live cells, strains were grown overnight in a rotator at 30°C in CM, diluted to
491 an OD_{600} of 0.1, and subcultured (30°C, CM, 300 RPM) for 4 hours before loading into an
492 Bioptechs FCS2 with a coverslip coated with 2% ConA to maintain desired temperature. All
493 OD_{600} measurements were taken with a GENESYS 20 spec with 1mL plastic cuvettes. For PB

494 imaging during heat shock (Fig 1. B-C, F-G & S1), cells were incubated in CM for 10 minutes at
495 46°C. For imaging PBs during starvation (Fig 1. D), SC5314 mNeonGreen tagged strains were
496 incubated in PBS at room temperature for 3 hours. To image PBs (Edc3-mNeonGreen) during
497 filamentation (Fig 1. E), we used 100% RPMI minus phenol red. All other filamentation assays
498 used RPMI supplemented with 10% FBS.

499 For spot plates, strains were grown overnight at 30°C in 5mL of liquid YPD on a rotator, diluted
500 to an OD_{600} of 0.5 and serially diluted 10-fold in YPD. YPD plates were spotted with 5µL of
501 diluted cells and incubated for 1-3 days at 30°C and 37°C prior to imaging with a Bio-Rad
502 ChemiDoc Touch Imaging System. To quantify growth in liquid YPD, strains were grown
503 overnight at 30°C in YPD on a rotator, diluted to an OD_{600} of 0.1 in 25mL YPD and incubated for
504 12 hours at 30°C. Strains were grown in triplicate andOD_{600} was measured hourly with a
505 GENESYS 20 visible spec with 1mL plastic cuvettes. Colony morphology under heat stress (4-
506 days, YPD, 37°C) and filamentation conditions (6-days, spider media, 37°C) was assayed
507 similarly prepared in the same manner. Strains were grown overnight in a rotator at 30°C in 3mL
508 liquid YPD, harvested by centrifugation (1,000 RCF, 5 minutes), washed three times with 6mL
509 PBS, and diluted to OD_{600} = 0.33 in 1mL PBS before spotting 3µL on YPD/spider plates.

510 To evaluate planktonic filamentation we grew strains overnight at 30°C in liquid YPD, diluted
511 them to an OD_{600} of 0.2 the following morning and subcultured them to an OD_{600} of 0.6 in 25mL
512 YPD before centrifuging (2,800 RCF, 5 minutes) the entire volume. We washed the cell pellet
513 with 5mL RPMI + 10% FBS and induced filamentation (25mL RPMI + 10% FBS, 37°C, 300
514 RPM). After 4 and 16 hours, cells were centrifuged (2,800 RCF, 5 minutes), fixed with 2mL 4%
515 formalin, and washed three times with 2mL PBS. 500µL of the washed cells in PBS were
516 stained the sample with 200µg/mL calcofluor white. The fixed and stained cells were allowed to
517 adhere to a glass slide treated with polyallylamine (PA) and washed with PBS prior to imaging

518 To survey biofilm growth, we grew cells overnight at 30°C in 5mL YPD on a rotator and diluted
519 them to an OD_{600} of 0.33 in 1.5mL RPMI + 10% serum. In four wells 200µL of diluted cells were
520 added to a 96-well ibidi plate coated with polyallylamine (PA) and incubated for 90-minutes at
521 37ºC for adherence. After 90 minutes, the media was removed leaving only adherent cells and
522 incubated with 400µL fresh RPMI + 10% serum. After a 24-hour incubation at 37°C, cells were
523 fixed with 350µL 4% formalin, washed twice with 400µL PBS, and stained with 400µL ConA
524 Alexa Fluor 594 conjugate (200µg/mL) overnight. The following morning we removed the ConA
525 Alexa Fluor 594 conjugate and washed the stained biofilms with 400µL PBS prior to adding
526 400µL 50% TDE in PBS and incubating it for 30 minutes. The 50% TDE solution was removed
527 and 400µL100% TDE solution was applied before confocal imaging.

528 Colony morphology under heat stress (4-days, YPD, 37°C) and filamentation conditions (6-days,
529 spider media, 37°C) was assayed similarly. Strains were grown overnight in a rotator at 30°C in
530 3mL liquid YPD, harvested by room temperature centrifugation (1,000 RCF, 5 minutes), washed
531 three times with 6mL PBS, and diluted to OD_{600} = 0.33 in 1mL PBS before spotting 3µL on
532 YPD/spider plates.

533 **Imaging and processing**

534 Single-cell fluorescence, DIC, and transmitted light images were captured with a Zeiss Axiovert
535 200M microscope using a 100X Plan-NEOFLUAR, 25X Plan-Apochromat, or 40X Plan-
536 Apochromat objective. For PB images in Fig. 1, all of the strains were in a SC5313 background
537 and imaged live. Temperature was maintained on the stage using a Bioptechs FCS2 chamber.
538 Only Fig 1. D is a confocal image captured with a 50-micron confocal slit wheel and processed
539 with a Z-projection. The remaining images in Fig. 1 consist of single planes of transmitted light
540 and fluorescence. As such, we were unable to quantify PB number or volume per cell in those
541 images. PB images in Fig. 1 were processed in Fiji by applying the Find Edges tool in the
542 transmitted light images for cell outlines, and background blur was reduced in the fluorescence

543 images using Subtract Background with a rolling ball radius of 30 pixels. Transmitted and
544 fluorescence images were overlaid using the Merge Channels tools. Replicates of the dual
545 labeled strain (Edc3-mNG, Dhh1-mS) are in Fig S1. A in addition to condensates in Dhh1-mS,
546 *edc3Δ/Δ* (Fig S1. B) and Edc3-mNG, *dhh1Δ/Δ* (Fig S1, C).

547 Spot plate images were adjusted for brightness/contrast in Fiji for increased visibility (Fig 2. A-B,
548 Fig 7. A, Fig S2. A). For the colonies under heat stress (4-days, YPD, 37°C) and filamentation
549 conditions (6-days, spider media, 37°C), images were collected with a Wild M8 Heerbrugg
550 Stereo Microscope at 6X and 25X and an iPhone 11 (Fig 2. D, Fig 4. E, Fig 7. C-D, Fig S2. F).
551 In Fiji colony images were converted to 8-bit and the LUT was inverted to improve resolution of
552 colony texture. To ensure comparability of colony size all 6X images were cropped to 1,500
553 pixels^2 and 25X images were cropped to 1,900 pixels^2 without any resizing. From DIC images in
554 Fig 2. E, cell and vacuole areas were measured in Fiji using the freehand tool in the Regions of
555 Interest (ROI) manager. A total of 100 cells across at least 4 fields of view were quantified to
556 generate the graphs Fig 2. F-H.

557 For the 4 and 16 hour planktonic filamentation assays we imaged short fluorescence confocal
558 stacks (Fig 3. A, C, Fig S2. B). In Fiji background blur was reduced in the fluorescence images
559 using Subtract Background with a rolling ball radius of 30 pixels prior to Z projection. We
560 quantified the extent of filamentation by measuring length by width in 100 cells in at least 4
561 fields of view using the straight and segmented line tools in the Regions of Interest (ROI)
562 manager (Fig 3. B, D, Fig S2. C).

563 For the biofilm growth assays, we took 25X fluorescence confocal stacks from the base to the
564 apical region of the biofilm (Fig 4. A, Fig S2. D). In Fiji we converted the images to 32 bit and
565 subtracted the background with a rolling ball radius of 13 pixels and set any resulting negative
566 values to zero. To generate a side view of the biofilm we resliced the rectified image, Z

567 projected and rescaled the Y values. The depth of the biofilms was quantified using the straight
568 line tool in the Regions of Interest (ROI) manager (Fig 4. B, Fig S2. E). To estimate cell density
569 throughout the biofilm we used pixel brightness as a proxy from the Plot Z-Axis Profile function
570 that generates a mean brightness (of the cell wall stain) for each slice in the stack (Fig 4. D).

571 **RNA-extraction and sequencing**

572 All experimental strains and conditions were assayed in triplicate (SC5314 WT YPD, SC5314
573 WT RPMI, SC5314 *dhh1Δ/Δ* YPD, SC5314 *dhh1Δ/Δ* RPMI) and (P57055 WT YPD, P57055 WT
574 RPMI, P57055 *dhh1Δ/Δ* YPD, P57055 *dhh1Δ/Δ* RPMI) for a total of 12 samples in each strain
575 background. Strains were grown overnight at 30°C in liquid YPD and diluted to an OD_{600} of 0.2
576 in liquid YPD the next morning. Sub-cultured cells were grown in 120mL YPD at 30°C with 300
577 RPM shaking until the OD_{600} reached 0.8. 20mL of the culture was collected in a 50mL falcon
578 tube and centrifuged at 4°C (3,220 RCF, 3 minutes). The supernatant was removed and the
579 cells were frozen at -80°C. 80mL of yeast cells were washed with PBS and resuspended in
580 80mL pre-warmed RPMI + 10% serum, followed by incubation at 37°C and 300 RPM. After 4
581 hours, 20mL of early hyphae was collected by sterile filtration (500mL Nalgene Rapid-Flow
582 Sterile Disposable Filter Unit with PES 0.2 µm), washed on the filter twice with 5mL ice cold
583 RNA buffer (4M NaCl, 1MTris-HCl pH7.5, EDTA), and frozen at -80°C. Cell pellets were stored
584 at -80°C.

585 RNA extraction was adapted from Cravener and Mitchell, 2020 [60]. Frozen cells in falcon tubes
586 were resuspended in 1mL ice-cold RNA buffer (4M NaCl, 1MTris-HCl pH7.5, EDTA). 500 uL of
587 resuspended cells were mixed with 250µL zirconia beads and 500 uL acid phenol:chloroform
588 pH4.5 (Ambion #AM9722) in 2mL microcentrifuge tubes and subjected to 10 cycles of vortexing
589 and chilling on ice for one minute each. After centrifugation at room temperature (16,873 RCF, 2
590 minutes), the aqueous phase was removed and back-extracted with an equal volume of
591 chloroform-isoamyl alcohol 24:1 (Sigma Aldrich #C0549). The resulting aqueous phase was

592 removed again, added to 3 volumes of ice cold 100% ethanol and precipitated at -80°C
593 overnight. The precipitated RNA was centrifuged at 4°C (20,817 RCF, 15 minutes) . RNA pellets
594 were washed with 1,800µL 70% ice cold ethanol and resuspended in 100µL ultrapure water.
595 Total RNA was quantified with a Thermo Scientific NanoDrop. Genomic DNA was removed from
596 5µg RNA using the invitrogen TURBO DNA-free kit according to manufacturer's specifications.
597 After the DNase treatment, RNA was re-extracted by adding 250µL RNA buffer, 500µL TRizol
598 (Invitrogen #15596026), and 250µL chloroform-isoamyl alcohol 24:1 (Sigma Aldrich #C0549).
599 This was vortexed and centrifuged at 4°C(20,817 RCF, 15 minutes). The aqueous phase was
600 removed and added to an equal volume of 100% ice cold ethanol and recovered using the RNA
601 Clean & Concentrator kit from Zymo Research according to the manufacturers specifications.
602 RNA was eluted in 60µL ultrapure water. RNA concentrations (range = 62.6ng/µL-105.5ng/µL)
603 were measured by NanoDrop and RIN^e was quantified using an Agilent 2200 TapeStation
604 System (range = $7.8RIN^e$ -$9.9RIN^e$). Strand-specific,150bp-paired ends were sequenced by
605 Novogene using the NEBNext Poly(A) mRNA Magnetic Isolation Module (NEB #E7490) to
606 isolate mRNA and the NEBNext Ultra II Directional RNA Library Prep Kit for Illumina (NEB
607 #E7760S/L) and sequenced an Illumina NovaSeq X-Plus Platform.

608 **Transcript alignment, quantification, and quality control**

609 Reads were aligned to the diploid *C. albicans* genome release 22 using HISAT2 version 2.2.1
610 [98] with the options (--known-splicesite-infile --rna-strandness R --max-intronlen 1400).
611 SAMTools version 1.15.1 [99] used to select and sort primary hits (samtools sort), generate a
612 bam.bai index (samtools index) and deeptools was used to generate positive (bamCoverage --
613 normalizeUsing BPM --exactScaling -bs 1 --filterRNAstrand=forward) and negative
614 (bamCoverage --normalizeUsing BPM --exactScaling -bs 1 --filterRNAstrand=reverse) strand
615 specific bigWig coverage tracks for IGV version 2.8.2 [100]. For each background, we quantified
616 the number of transcripts in each strain (WT, *dhh1Δ/Δ*) and growth condition (YPD, RPMI) with

617 the coverageBed function of BEDTools version 2.30.0 [101]. All 12 experimental groups for
618 SC5314 and P57055 were combined into a single file of raw hits for each strain (Tables S10-
619 11). Our aligned read depth ranged from 18.6 million (P57055 WT, RPMI) to 37.5 million
620 (SC5314 dhh1Δ/Δ, RPMI) aligned reads with a mean aligned read depth of 26.6 million.

621 For quality control, coverage tracks of select genes are shown in Fig. S4. We confirmed that
622 *DHH1* transcripts were present in WT cells and absent in *dhh1Δ/Δ* under both growth conditions
623 with IGV (Fig S3. A). Using R version 4.3.1 and the edgeR release 3.20 [102] package we
624 converted raw hits to copies to million (Fig S8. A). Poorly transcribed ORFs (<1 Counts Per
625 Million (CPM) in <3 groups) were screened out leaving only hits with ≥1 CPM in ≥ 3 groups (Fig
626 S8. B). Using the built-in R function prcomp we performed a principal component analysis,
627 confirming replicates are clustered by strain and growth conditions (Fig S9. A-B). The filtered
628 CPM hits were analyzed with DEseq2 release 3.20 [61] with a Padj-value cutoff of 0.01 for strict
629 identification of differentially expressed genes.

630 **GO analysis**

631 For the GO term analysis of DE genes we focused on transcripts that were differentially
632 expressed with a $Log_2FC > +2.5$ or < -2.5 in Figs. 5, 6, S4, and S5. However, due to the smaller
633 number of transcripts DE in the same direction in both SC5314 and P57055 we selected
634 transcripts with a $Log_2FC > +1.0$ or < -1.0 for Fig 8. The analysis was performed in the *Candida*
635 Genome Database [103] CGD Gene Ontology Term Finder (http://www.candidagenome.org/cgi-
636 bin/GO/goTermFinder). Only terms with a corrected P-value of < 0.1 are generated with this
637 tool. However, we selected a maximum of 10 terms with the greatest fold enrichment, an
638 overwhelming majority of which had a Padj < 0.01 from the GO analysis.

639 **Software and data analysis**

640 All images were processed with Fiji [104]. Primers and transformation cassettes were designed
641 using sequences from the *Candida* Genome Database [103] and the *Candida albicans* Umbrella

642 Comparative genomics project [58], NCBI bioproject ID: PRJNA193498. Codon adaptation
643 index (CAI) was calculated using CAIcal [105] and codon usage table from the *Candida*
644 Genome database [103]. Data analysis and statistical tests were performed using GraphPad
645 Prism version 10.0.0 for Windows [106] as well as R version 4.3.1 [107] with ggplot2 3.5.1 [108]
646 and bioconductor packages release 3.20 including edgeR [102] and DESeq2 [61]. We used
647 Affinity Designer for Windows Version 2.5.5, 2024and BioRender.com to compose our figures.

648 **Data accessibility**

649 Raw RNA-seq data have been deposited at the NCBI SRA under bioproject number
650 PRJNA1133750 A GEO submission is also available under accession GSE284543. All other
651 data are provided in the supplemental tables.

652 **Acknowledgements**

653 We would like to thank Gemma E. May for her cloning expertise and support as well as the
654 members of the McManus laboratory for helpful discussions.

655

656 **References**

657 [1] Brown GD, Denning DW, Gow NAR, et al. Hidden killers: human fungal infections. *Sci*
658 *Transl Med* 2012; 4: 165rv13.

659 [2] Kullberg BJ, Arendrup MC. Invasive Candidiasis. *N Engl J Med* 2015; 373: 1445–1456.

660 [3] Kadosh D, Lopez-Ribot JL. Candida albicans: adapting to succeed. *Cell Host Microbe*
661 2013; 14: 483–485.

662 [4] Brown AJP, Budge S, Kaloriti D, et al. Stress adaptation in a pathogenic fungus. *J Exp Biol*
663 2014; 217: 144–155.

664 [5] Moyes DL, Wilson D, Richardson JP, et al. Candidalysin is a fungal peptide toxin critical for
665 mucosal infection. *Nature* 2016; 532: 64–68.

666 [6] Desai JV, Mitchell AP. Candida albicans Biofilm Development and Its Genetic Control.
667 *Microbiol Spectr*; 3. Epub ahead of print June 2015. DOI: 10.1128/microbiolspec.MB-0005-
668 2014.

669 [7] Finkel JS, Mitchell AP. Genetic control of Candida albicans biofilm development. *Nat Rev*

670 *Microbiol* 2011; 9: 109–118.

671 [8] Chandra Jyotsna, Kuhn Duncan M., Mukherjee Pranab K., et al. Biofilm Formation by the
672 Fungal Pathogen Candida albicans: Development, Architecture, and Drug Resistance. *J*
673 *Bacteriol* 2001; 183: 5385–5394.

674 [9] Villa S, Hamideh M, Weinstock A, et al. Transcriptional control of hyphal morphogenesis in
675 Candida albicans. *FEMS Yeast Res*; 20. Epub ahead of print 1 February 2020. DOI:
676 10.1093/femsyr/foaa005.

677 [10] Chen H, Zhou X, Ren B, et al. The regulation of hyphae growth in Candida albicans.
678 *Virulence* 2020; 11: 337–348.

679 [11] Martin R, Albrecht-Eckardt D, Brunke S, et al. A core filamentation response network in
680 Candida albicans is restricted to eight genes. *PLoS One* 2013; 8: e58613.

681 [12] Glazier VE. EFG1, Everyone's Favorite Gene in Candida albicans: A Comprehensive
682 Literature Review. *Front Cell Infect Microbiol* 2022; 12: 855229.

683 [13] Azadmanesh J, Gowen AM, Creger PE, et al. Filamentation Involves Two Overlapping, but
684 Distinct, Programs of Filamentation in the Pathogenic Fungus Candida albicans.

685 [14] Huang MY, Woolford CA, May G, et al. Circuit diversification in a biofilm regulatory network.
686 *PLoS Pathog* 2019; 15: e1007787.

687 [15] Kadosh D. Control of Candida albicans morphology and pathogenicity by post-
688 transcriptional mechanisms. *Cell Mol Life Sci* 2016; 73: 4265–4278.

689 [16] Verma-Gaur J, Traven A. Post-transcriptional gene regulation in the biology and virulence
690 of Candida albicans. *Cell Microbiol* 2016; 18: 800–806.

691 [17] Pizzinga M, Harvey RF, Garland GD, et al. The cell stress response: extreme times call for
692 post-transcriptional measures. *Wiley Interdiscip Rev RNA* 2020; 11: e1578.

693 [18] Hernández-Elvira M, Sunnerhagen P. Post-transcriptional regulation during stress. *FEMS*
694 *Yeast Res*; 22. Epub ahead of print 30 June 2022. DOI: 10.1093/femsyr/foac025.

695 [19] Keene JD. RNA regulons: coordination of post-transcriptional events. *Nat Rev Genet* 2007;
696 8: 533–543.

697 [20] Halbeisen RE, Galgano A, Scherrer T, et al. Post-transcriptional gene regulation: from
698 genome-wide studies to principles. *Cell Mol Life Sci* 2008; 65: 798–813.

699 [21] Bloom ALM, Leipheimer J, Panepinto JC. mRNA decay: an adaptation tool for the
700 environmental fungal pathogen Cryptococcus neoformans. *Wiley Interdiscip Rev RNA*; 8.
701 Epub ahead of print September 2017. DOI: 10.1002/wrna.1424.

702 [22] Rana A, Gupta N, Thakur A. Post-transcriptional and translational control of the morphology
703 and virulence in human fungal pathogens. *Mol Aspects Med* 2021; 81: 101017.

704 [23] Balagopal V, Parker R. Polysomes, P bodies and stress granules: states and fates of
705 eukaryotic mRNAs. *Curr Opin Cell Biol* 2009; 21: 403–408.

706 [24] Youn J-Y, Dyakov BJA, Zhang J, et al. Properties of Stress Granule and P-Body
707 Proteomes. *Mol Cell* 2019; 76: 286–294.

708 [25] Mugler CF, Hondele M, Heinrich S, et al. ATPase activity of the DEAD-box protein Dhh1
709 controls processing body formation. *Elife*; 5. Epub ahead of print 3 October 2016. DOI:
710 10.7554/eLife.18746.

711 [26] Collart MA. The Ccr4-Not complex is a key regulator of eukaryotic gene expression. *Wiley*
712 *Interdiscip Rev RNA* 2016; 7: 438–454.

713 [27] Teixeira D, Sheth U, Valencia-Sanchez MA, et al. Processing bodies require RNA for
714 assembly and contain nontranslating mRNAs. *RNA* 2005; 11: 371–382.

715 [28] Protter DSW, Parker R. Principles and Properties of Stress Granules. *Trends Cell Biol*
716 2016; 26: 668–679.

717 [29] Dagley MJ, Gentle IE, Beilharz TH, et al. Cell wall integrity is linked to mitochondria and
718 phospholipid homeostasis in Candida albicans through the activity of the post-
719 transcriptional regulator Ccr4-Pop2. *Mol Microbiol* 2011; 79: 968–989.

720 [30] Cheng S, Clancy CJ, Checkley MA, et al. Identification of Candida albicans genes induced
721 during thrush offers insight into pathogenesis. *Mol Microbiol* 2003; 48: 1275–1288.

722 [31] Cheng S, Nguyen MH, Zhang Z, et al. Evaluation of the roles of four Candida albicans
723 genes in virulence by using gene disruption strains that express URA3 from the native
724 locus. *Infect Immun* 2003; 71: 6101–6103.

725 [32] Cheng S, Clancy CJ, Checkley MA, et al. The role of Candida albicans NOT5 in virulence
726 depends upon diverse host factors in vivo. *Infect Immun* 2005; 73: 7190–7197.

727 [33] Richard ML, Nobile CJ, Bruno VM, et al. Candida albicans biofilm-defective mutants.
728 *Eukaryot Cell* 2005; 4: 1493–1502.

729 [34] An H-S, Lee K-H, Kim J. Identification of an exoribonuclease homolog, CaKEM1/CaXRN1,
730 in Candida albicans and its characterization in filamentous growth. *FEMS Microbiol Lett*
731 2004; 235: 297–303.

732 [35] Shively CA, Kweon HK, Norman KL, et al. Large-Scale Analysis of Kinase Signaling in
733 Yeast Pseudohyphal Development Identifies Regulation of Ribonucleoprotein Granules.
734 *PLoS Genet* 2015; 11: e1005564.

735 [36] Jung J-H, Kim J. Accumulation of P-bodies in Candida albicans under different stress and
736 filamentous growth conditions. *Fungal Genet Biol* 2011; 48: 1116–1123.

737 [37] Jung J-H, Kim J. Roles of Edc3 in the oxidative stress response and CaMCA1-encoded
738 metacaspase expression in Candida albicans. *FEBS J* 2014; 281: 4841–4851.

739 [38] Raser JM, O'Shea EK. Noise in gene expression: origins, consequences, and control.
740 *Science* 2005; 309: 2010–2013.

741 [39] Zhuravel D, Fraser D, St-Pierre S, et al. Phenotypic impact of regulatory noise in cellular
742 stress-response pathways. *Syst Synth Biol* 2010; 4: 105–116.

743 [40] Urban EA, Johnston RJ Jr. Buffering and Amplifying Transcriptional Noise During Cell Fate
744 Specification. *Front Genet* 2018; 9: 591.

745 [41] Timmers HTM, Tora L. Transcript Buffering: A Balancing Act between mRNA Synthesis and
746 mRNA Degradation. *Mol Cell* 2018; 72: 10–17.

747 [42] Palenchar PM, DeStefanis T. Transcriptional noise adjusted for expression levels reveals
748 genes with high transcriptional noise that are highly expressed, functionally related, and co-
749 regulated in yeast. *Curr Genet* 2022; 68: 675–686.

750 [43] Nissan T, Rajyaguru P, She M, et al. Decapping activators in Saccharomyces cerevisiae
751 act by multiple mechanisms. *Mol Cell* 2010; 39: 773–783.

752 [44] Rao BS, Parker R. Numerous interactions act redundantly to assemble a tunable size of P
753 bodies in Saccharomyces cerevisiae. *Proc Natl Acad Sci U S A* 2017; 114: E9569–E9578.

754 [45] Carroll JS, Munchel SE, Weis K. The DExD/H box ATPase Dhh1 functions in translational
755 repression, mRNA decay, and processing body dynamics. *J Cell Biol* 2011; 194: 527–537.

756 [46] Sweet T, Kovalak C, Coller J. The DEAD-box protein Dhh1 promotes decapping by slowing
757 ribosome movement. *PLoS Biol* 2012; 10: e1001342.

758 [47] Radhakrishnan A, Chen Y-H, Martin S, et al. The DEAD-Box Protein Dhh1p Couples
759 mRNA Decay and Translation by Monitoring Codon Optimality. *Cell* 2016; 167: 122–
760 132.e9.

761 [48] Vijjamarri AK, Gupta N, Onu C, et al. mRNA decapping activators Pat1 and Dhh1 regulate
762 transcript abundance and translation to tune cellular responses to nutrient availability.
763 *Nucleic Acids Res* 2023; 51: 9314–9336.

764 [49] Park Y-U, Hur H, Ka M, et al. Identification of translational regulation target genes during
765 filamentous growth in Saccharomyces cerevisiae: regulatory role of Caf20 and Dhh1.
766 *Eukaryot Cell* 2006; 5: 2120–2127.

767 [50] Ka M, Park Y-U, Kim J. The DEAD-box RNA helicase, Dhh1, functions in mating by
768 regulating Ste12 translation in Saccharomyces cerevisiae. *Biochem Biophys Res Commun*
769 2008; 367: 680–686.

770 [51] Park Y-D, Panepinto J, Shin S, et al. Mating pheromone in Cryptococcus neoformans is
771 regulated by a transcriptional/degradative 'futile' cycle. *J Biol Chem* 2010; 285: 34746–
772 34756.

773 [52] Lee E, Jung D, Kim J. Roles of Dhh1 RNA helicase in yeast filamentous growth: Analysis of
774 N-terminal phosphorylation residues and ATPase domains. *J Microbiol* 2020; 58: 853–858.

775 [53] Kshirsagar M, Parker R. Identification of Edc3p as an enhancer of mRNA decapping in
776 Saccharomyces cerevisiae. *Genetics* 2004; 166: 729–739.

777 [54] Kumar R, Zhang F, Niphadkar S, et al. Decapping activators Edc3 and Scd6 act
778 redundantly with Dhh1 in post-transcriptional repression of starvation-induced pathways.
779 *bioRxivorg*. Epub ahead of print 28 August 2024. DOI: 10.1101/2024.08.28.610059.

780 [55] Decker CJ, Teixeira D, Parker R. Edc3p and a glutamine/asparagine-rich domain of Lsm4p

781 function in processing body assembly in Saccharomyces cerevisiae. *J Cell Biol* 2007; 179:
782 437–449.

783 [56] Wang C-Y, Chen W-L, Wang S-W. Pdc1 functions in the assembly of P bodies in
784 Schizosaccharomyces pombe. *Mol Cell Biol* 2013; 33: 1244–1253.

785 [57] Huang MY, Cravener MC, Mitchell AP. Targeted Genetic Changes in Candida albicans
786 Using Transient CRISPR-Cas9 Expression. *Curr Protoc* 2021; 1: e19.

787 [58] Hirakawa MP, Martinez DA, Sakthikumar S, et al. Genetic and phenotypic intra-species
788 variation in Candida albicans. *Genome Res* 2015; 25: 413–425.

789 [59] Xing W, Muhlrad D, Parker R, et al. A quantitative inventory of yeast P body proteins
790 reveals principles of composition and specificity. *Elife*; 9. Epub ahead of print 19 June 2020.
791 DOI: 10.7554/eLife.56525.

792 [60] Cravener MV, Mitchell AP. Candida albicans culture, cell harvesting, and total RNA
793 extraction. *Bio Protoc* 2020; 10: e3803.

794 [61] Love MI, Huber W, Anders S. Moderated estimation of fold change and dispersion for RNA-
795 seq data with DESeq2. *Genome Biol* 2014; 15: 550.

796 [62] Murad A, Leng P, Straffon M, et al. NRG1 represses yeast–hypha morphogenesis and
797 hypha-specific gene expression in Candida albicans. *EMBO J*; 20. Epub ahead of print 3
798 September 2001. DOI: 10.1093/emboj/20.17.4742.

799 [63] Braun BR, Kadosh D, Johnson AD. NRG1, a repressor of filamentous growth in C.albicans,
800 is down-regulated during filament induction. *EMBO J*; 20.

801 [64] LaFayette SL, Collins C, Zaas AK, et al. PKC signaling regulates drug resistance of the
802 fungal pathogen Candida albicans via circuitry comprised of Mkc1, calcineurin, and Hsp90.
803 *PLoS Pathog* 2010; 6: e1001069.

804 [65] Xie JL, Qin L, Miao Z, et al. The Candida albicans transcription factor Cas5 couples stress
805 responses, drug resistance and cell cycle regulation. *Nat Commun* 2017; 8: 499.

806 [66] Bruno VM, Wang Z, Marjani SL, et al. Comprehensive annotation of the transcriptome of
807 the human fungal pathogen Candida albicans using RNA-seq. *Genome Res* 2010; 20:
808 1451–1458.

809 [67] Carlisle PL, Kadosh D. A genome-wide transcriptional analysis of morphology
810 determination in Candida albicans. *Mol Biol Cell* 2013; 24: 246–260.

811 [68] Kadosh D, Johnson AD. Induction of the Candida albicans Filamentous Growth Program by
812 Relief of Transcriptional Repression: A Genome-wide Analysis. *carried out (Odds* 2004;
813 1985: 1988.

814 [69] Wakade RS, Wellington M, Krysan DJ. Temporal dynamics of Candida albicans
815 morphogenesis and gene expression reveals distinctions between in vitro and in vivo
816 filamentation. *mSphere* 2024; e0011024.

817 [70] Nantel A, Dignard D, Bachewich C, et al. Transcription profiling of Candida albicans cells
818 undergoing the yeast-to-hyphal transition. *Mol Biol Cell* 2002; 13: 3452–3465.

819 [71] Nobile CJ, Fox EP, Nett JE, et al. A recently evolved transcriptional network controls biofilm
820 development in Candida albicans. *Cell* 2012; 148: 126–138.

821 [72] Enjalbert B, Nantel A, Whiteway M. Stress-induced gene expression in Candida albicans:
822 absence of a general stress response. *Mol Biol Cell* 2003; 14: 1460–1467.

823 [73] Cravener MV, Do E, May G, et al. Reinforcement amid genetic diversity in the Candida
824 albicans biofilm regulatory network. *PLoS Pathog* 2023; 19: e1011109.

825 [74] Cleary IA, Lazzell AL, Monteagudo C, et al. BRG1 and NRG1 form a novel feedback circuit
826 regulating Candida albicans hypha formation and virulence. *Mol Microbiol* 2012; 85: 557–
827 573.

828 [75] Banerjee M, Thompson DS, Lazzell A, et al. UME6, a novel filament-specific regulator of
829 Candida albicans hyphal extension and virulence. *Mol Biol Cell* 2008; 19: 1354–1365.

830 [76] Dong S, Li C, Zenklusen D, et al. YRA1 autoregulation requires nuclear export and
831 cytoplasmic Edc3p-mediated degradation of its pre-mRNA. *Mol Cell* 2007; 25: 559–573.

832 [77] He F, Li C, Roy B, et al. Yeast Edc3 targets RPS28B mRNA for decapping by binding to a
833 3' untranslated region decay-inducing regulatory element. *Mol Cell Biol* 2014; 34: 1438–
834 1451.

835 [78] Wellington M, Rustchenko E. 5-Fluoro-orotic acid induces chromosome alterations in
836 Candida albicans. *Yeast* 2005; 22: 57–70.

837 [79] Lay J, Henry LK, Clifford J, et al. Altered expression of selectable marker URA3 in gene-
838 disrupted Candida albicans strains complicates interpretation of virulence studies. *Infect*
839 *Immun* 1998; 66: 5301–5306.

840 [80] Brand Alexandra, MacCallum Donna M., Brown Alistair J. P., et al. Ectopic Expression of
841 URA3 Can Influence the Virulence Phenotypes and Proteome of Candida albicans but Can
842 Be Overcome by Targeted Reintegration of URA3 at the RPS10 Locus. *Eukaryot Cell* 2004;
843 3: 900–909.

844 [81] Vijjamarri AK, Niu X, Vandermeulen MD, et al. Decapping factor Dcp2 controls mRNA
845 abundance and translation to adjust metabolism and filamentation to nutrient availability.
846 *Elife*; 12. Epub ahead of print 2 June 2023. DOI: 10.7554/eLife.85545.

847 [82] Matheny T, Rao BS, Parker R. Transcriptome-Wide Comparison of Stress Granules and P-
848 Bodies Reveals that Translation Plays a Major Role in RNA Partitioning. *Mol Cell Biol*; 39.
849 Epub ahead of print 15 December 2019. DOI: 10.1128/MCB.00313-19.

850 [83] Kim E-C, Kim J. Deletion analysis of LSm, FDF, and YjeF domains of Candida albicans
851 Edc3 in hyphal growth and oxidative-stress response. *J Microbiol* 2015; 53: 111–115.

852 [84] Dunn MJ, Fillinger RJ, Anderson LM, et al. Automated quantification of Candida albicans
853 biofilm-related phenotypes reveals additive contributions to biofilm production. *NPJ Biofilms*
854 *Microbiomes* 2020; 6: 36.

855 [85] Brandquist ND, Lampman C, Smith EJ, et al. Significant variation of filamentation
856 phenotypes in clinical Candida albicans strains. *Front Cell Infect Microbiol*; 13. Epub ahead
857 of print 2023. DOI: 10.3389/fcimb.2023.1207083.

858 [86] Desai JV, Cheng S, Ying T, et al. Coordination of Candida albicans Invasion and Infection
859 Functions by Phosphoglycerol Phosphatase Rhr2. *Pathogens* 2015; 4: 573–589.

860 [87] Staab JF, Bradway SD, Fidel PL, et al. Adhesive and mammalian transglutaminase
861 substrate properties of Candida albicans Hwp1. *Science* 1999; 283: 1535–1538.

862 [88] Childers DS, Mundodi V, Banerjee M. A 5′ UTR-mediated translational efficiency
863 mechanism inhibits the Candida albicans morphological transition. *Molecular*,
864 https://onlinelibrary.wiley.com/doi/abs/10.1111/mmi.12576 (2014).

865 [89] Pierce JV, Kumamoto CA. Variation in Candida albicans EFG1 expression enables host-
866 dependent changes in colonizing fungal populations. *MBio* 2012; 3: e00117–12.

867 [90] Bloom ALM, Panepinto JC. RNA biology and the adaptation of Cryptococcus neoformans to
868 host temperature and stress. *Wiley Interdiscip Rev RNA* 2014; 5: 393–406.

869 [91] Panepinto J, Liu L, Ramos J, et al. The DEAD-box RNA helicase Vad1 regulates multiple
870 virulence-associated genes in Cryptococcus neoformans. *J Clin Invest* 2005; 115: 632–641.

871 [92] Milholland KL, Gregor JB, Hoda S, et al. Rapid, efficient auxin-inducible protein degradation
872 in Candida pathogens. *mSphere* 2023; 8: e0028323.

873 [93] Cihlar RL, Calderone RA. Candida albicans: methods and protocols. Preface. *Methods Mol*
874 *Biol* 2009; 499: v.

875 [94] Sasse C, Morschhäuser J. Gene deletion in Candida albicans wild-type strains using the
876 SAT1-flipping strategy. *Methods Mol Biol* 2012; 845: 3–17.

877 [95] Frazer C, Hernday AD, Bennett RJ. Monitoring Phenotypic Switching in Candida albicans
878 and the Use of Next-Gen Fluorescence Reporters. *Curr Protoc Microbiol* 2019; 53: e76.

879 [96] Vyas VK, Barrasa MI, Fink GR. A Candida albicans CRISPR system permits genetic
880 engineering of essential genes and gene families. *Sci Adv* 2015; 1: e1500248.

881 [97] Hoffman CS. Preparation of yeast DNA. *Curr Protoc Mol Biol* 2001; Chapter 13: Unit13.11.

882 [98] Kim D, Paggi JM, Park C, et al. Graph-based genome alignment and genotyping with
883 HISAT2 and HISAT-genotype. *Nat Biotechnol* 2019; 37: 907–915.

884 [99] Danecek P, Bonfield JK, Liddle J, et al. Twelve years of SAMtools and BCFtools.
885 *Gigascience*; 10. Epub ahead of print 16 February 2021. DOI:
886 10.1093/gigascience/giab008.

887 [100] Robinson JT, Thorvaldsdóttir H, Winckler W, et al. Integrative genomics viewer. *Nat*
888 *Biotechnol* 2011; 29: 24–26.

889 [101] Quinlan AR, Hall IM. BEDTools: a flexible suite of utilities for comparing genomic
890 features. *Bioinformatics* 2010; 26: 841–842.

891 [102] Robinson MD, McCarthy DJ, Smyth GK. edgeR: a Bioconductor package for differential
892 expression analysis of digital gene expression data. *Bioinformatics* 2010; 26: 139–140.

893 [103] Skrzypek MS, Binkley J, Sherlock G. Using the Candida Genome Database. *Methods*

894 *Mol Biol* 2018; 1757: 31–47.

895 [104] Schindelin J, Arganda-Carreras I, Frise E, et al. Fiji: an open-source platform for
896 biological-image analysis. *Nat Methods* 2012; 9: 676–682.

897 [105] Puigbò P, Bravo IG, Garcia-Vallve S. CAIcal: a combined set of tools to assess codon
898 usage adaptation. *Biol Direct* 2008; 3: 38.

899 [106] Swift ML. GraphPad Prism, Data Analysis, and Scientific Graphing. *J Chem Inf Comput*
900 *Sci* 1997; 37: 411–412.

901 [107] R Core Team. R: A Language and Environment for Statistical Computing, https://www.R-
902 project.org/ (2021).

903 [108] Wickham H. ggplot2: Elegant Graphics for Data Analysis, https://ggplot2.tidyverse.org
904 (2016).

905

906 ## Supporting Tables

907 **Table S1. DEseq2 results comparing SC5314 YPD *dhh1Δ/Δ* vs. SC5314 YPD WT for Fig 5. A.**
908 Exponentially growing *dhh1Δ/Δ* and WT SC5314 yeast cells in YPD at 30°C. RNA extraction performed in
909 triplicate from three separate samples.

910 **Table S2. DEseq2 results comparing SC5314 RPMI *dhh1Δ/Δ* vs. SC5314 RPMI WT for Fig 5. C.**
911 *dhh1Δ/Δ* and WT SC5314 grown under physiologically relevant filamentation conditions (RPMI + 10%
912 serum at 37°C) for 4 hours. RNA extraction performed in triplicate from three separate samples.

913 **Table S3. DEseq2 results comparing SC5314 RPMI WT vs SC5314 YPD WT for Fig 6. A.** WT SC5314
914 yeast cells in YPD at 30°C and WT SC5314 grown under physiologically relevant filamentation conditions
915 (RPMI + 10% serum at 37°C) for 4 hours. RNA extraction performed in triplicate from three separate
916 samples.

917 **Table S4. DEseq2 results comparing SC5314 RPMI *dhh1Δ/Δ* vs SC5314 YPD *dhh1Δ/Δ* for Fig 6. D.**
918 *dhh1Δ/Δ* yeast cells in YPD at 30°C and *dhh1Δ/Δ* grown under physiologically relevant filamentation
919 conditions (RPMI + 10% serum at 37°C) for 4 hours. RNA extraction performed in triplicate from three
920 separate samples.

921 **Table S5. DEseq2 results comparing P57055 YPD *dhh1Δ/Δ* vs. P57055 YPD WT for Fig S4. A.**
922 Exponentially growing *dhh1Δ/Δ* and WT P57055 yeast cells in YPD at 30°C. RNA extraction performed in
923 triplicate from three separate samples.

924 **Table S6. DEseq2 results comparing P57055 RPMI *dhh1Δ/Δ* vs. P57055 RPMI WT for Fig S4. C.**
925 *dhh1Δ/Δ* and WT P57055 grown under physiologically relevant filamentation conditions (RPMI + 10%
926 serum at 37°C) for 4 hours. RNA extraction performed in triplicate from three separate samples.

927 **Table S7. DEseq2 results comparing P57055 RPMI WT vs P57055 YPD WT for Fig S5. A.** WT
928 P57055 yeast cells in YPD at 30°C and WT P57055 grown under physiologically relevant filamentation
929 conditions (RPMI + 10% serum at 37°C) for 4 hours. RNA extraction performed in triplicate from three
930 separate samples.

931 **Table S8. DEseq2 results comparing P57055 RPMI *dhh1Δ/Δ* vs P57055 YPD *dhh1Δ/Δ* for Fig S5. D.**
932 *dhh1Δ/Δ* yeast cells in YPD at 30°C and *dhh1Δ/Δ* grown under physiologically relevant filamentation
933 conditions (RPMI + 10% serum at 37°C) for 4 hours. RNA extraction performed in triplicate from three
934 separate samples.

935 **Table S9. List of strains, plasmids, PAM sites, and primers used in this study.** This table includes
936 relevant information concerning our strain generation and validation.

937 **Table S10. Raw RNA-seq hits for SC5314 WT and *dhh1Δ/Δ i*n YPD and RPMI.** Unfiltered raw aligned
938 RNA-seq hits used for DEseq2 input.

939 **Table S11. Raw RNA-seq hits for P57055 WT and *dhh1Δ/Δ* in YPD and RPMI.** Unfiltered raw aligned
940 RNA-seq hits used for DEseq2 input.

941 **Table S12. Core genes differentially expressed in the same direction for YPD SC5314 *dhh1Δ/Δ* and**
942 **YPD P57057 *dhh1Δ/Δ*.** In YPD, both *dhh1Δ/Δ* strains had 457 genes downregulated (blue circles Fig 8.
943 A) and 632 genes upregulated (red circles Fig 8. A). Data from DEseq2 results in Tables S1 and S5.

944 **Table S13. Core genes differentially expressed in the same direction for RPMI SC5314 *dhh1Δ/Δ***
945 **and RPMI P57057 *dhh1Δ/Δ.*** In RPMI, both *dhh1Δ/Δ* strains had 883 genes downregulated (blue circles
946 Fig 8. D) and 901 genes upregulated (red circles Fig 8. D). Data from DEseq2 results in Tables S2 and
947 S6.

948